

Lappeenranta University of Technology  
LUT School of Energy Systems  
Degree Program in Electrical Engineering

Joni Siimesjärvi

**SENSORLESS DETECTION OF DELETERIOUS  
PHENOMENA IN PUMP AND FAN SYSTEMS VIA  
VARIABLE SPEED DRIVE**

Examiners: D.Sc. Olli Alkkiomäki  
D.Sc. Tero Ahonen

## **ABSTRACT**

Lappeenranta University of Technology  
LUT School of Energy Systems  
Degree Program in Electrical Engineering

Joni Siimesjärvi

### **Sensorless detection of deleterious phenomena in pump and fan systems via variable speed drive**

2016

Master's Thesis  
Pages 71, figures 55, tables 8

Examiners: D.Sc. Olli Alkkiomäki  
Post-doctoral researcher Tero Ahonen

Keywords: variable speed drive, sensorless, cavitation, stall, contamination, pump, fan

Pump and fan systems consume a large portion of the total energy on a global scale. Variable speed drives are amongst the most efficient solutions to reduce energy consumption in fluid handling systems. More efficient system can also be achieved by detecting and reacting to efficiency reducing adverse phenomena present in the system. This can be done with system monitoring.

Traditional process monitoring is done by having sensors installed to measure desired variables. While sensors provide valuable information they can be replaced by having model-based estimates rather than actual physical measurements. Modern variable speed drives are capable of providing accurate estimates of variables such as power, torque and rotational speed. With these estimates a sensorless system monitoring can be realized to detect harmful phenomena. Remote monitoring can be implemented by having an access to the monitored data with either a direct connection to the variable speed drive or an access to a data logger connected to the drive. Alternatively the logger could forward the collected data to a server which is utilized by a monitoring software.

In this thesis sensorless methods to detect deleterious phenomena in fluid handling systems are presented. The studied phenomena are introduced, as well as their causes and effects on energy efficiency and life-cycle costs. Remote monitoring of a pump and a fan system are implemented in a laboratory environment to test applicability of the presented sensorless detection methods. A pilot experiment is included in which occurrence of cavitation is remotely monitored with sensorless detection methods.

## TIIVISTELMÄ

Lappeenrannan teknillinen yliopisto  
LUT Energiajärjestelmät  
Sähkötekniikan koulutusohjelma

Joni Siimesjärvi

### **Pumppu- ja puhallinjärjestelmien haitallisten ilmiöiden havaitseminen ilman antureita taajuusmuuttajan avulla** 2016

Diplomityö  
Sivumäärä 71, kuvia 55, taulukoita 8

Työn tarkastajat: TkT Olli Alkkiomäki  
Tutkijatohtori Tero Ahonen

Hakusanat: taajuusmuuttaja, anturiton, kavitaatio, sakkaus, likaantuminen, pumppu, puhallin,  
Keywords: variable speed drive, sensorless, cavitation, stall, contamination, pump, fan

Pumppu- ja puhallinjärjestelmät käyttävät suuren osan maailmanlaajuisesta kokonaisenergiankulutuksesta. Taajuusmuuttajat ovat yksi merkittävimpiä tapoja vähentää energian kulutusta näissä järjestelmissä. Energiaa voidaan myös käyttää tehokkaammin, jos voidaan havaita sekä vähentää käytönaikana ilmenevien haitallisten ilmiöiden vaikutusta. Tätä varten järjestelmän tilaa pitää pystyä tarkkailemaan.

Perinteinen prosessimonitorointi voidaan tehdä asentamalla antureita, jotka mittaavat haluttuja muuttujia. Vaikka antureilta saadaankin arvokasta tietoa, fyysisten mittausten sijaan voidaan soveltaa malleihin pohjautuvia muuttuja-arvioita. Modernit taajuusmuuttajat pystyvät antamaan tarkkoja arvioita mm. tehosta, vääntömomentista sekä pyörimisnopeudesta. Näiden arvioiden avulla järjestelmän monitorointi sekä haitallisten ilmiöiden havainnointi voidaan toteuttaa ilman antureita. Monitorointi voidaan toteuttaa myös etäältä, jos mittausdataan päästään käsiksi etäyhteydellä joko suoraan taajuusmuuttajan tai muuttajaan kiinnitetyn datankerääjän kautta. Vaihtoehtoisesti taajuusmuuttaja tai datankerääjä voisi lähettää mittausdataa suoraan palvelimelle, jota monitorointiohjelma pystyisi hyödyntämään.

Tässä diplomityössä esitellään tapoja havaita haitallisia ilmiöitä pumppu- ja puhallinjärjestelmistä ilman mittausantureita. Tutkittavat ilmiöt esitellään, kuten myös syyt niiden ilmenemiseen ja niiden vaikutukset järjestelmän energiatehokkuuteen sekä elinkaarikustannuksiin. Pumppu- ja puhallinjärjestelmän etämonitorointi toteutetaan laboratorio-olosuhteissa. Samalla testataan esiteltyjen anturittomien havainnointimenetelmien toimivuutta. Etämonitorointia ja anturittomia kavitoinnin havaitsemista sovelletaan laboratorion lisäksi myös pilottikohteessa.

## **PREFACE**

This thesis has been done on behalf of the Laboratory of Digital Systems and Control Engineering in Lappeenranta University of Technology (LUT). The thesis was part of Efficient Energy Use (EFEU) program, which focuses on developing new energy efficient solutions for fluid handling systems.

First I would like to thank Post-doctoral researcher Tero Ahonen for all the help he has provided throughout making of this thesis and my studies. I would also like to thank D.Sc. Olli Alkkio from ABB for providing the subject of this thesis and valuable feedback during the making process.

I want to thank my parents for lifetime of support and encouragement. You have helped me more than I can ever express. Lastly, I want to thank my friends who have made my time at LUT memorable.

Jaala, September 7<sup>th</sup>, 2016

Joni Siimesjärvi

# TABLE OF CONTENTS

<b>SYMBOLS AND ABBREVIATIONS.....</b>	<b>3</b>
<b>1 INTRODUCTION .....</b>	<b>4</b>
1.1 OBJECTIVE OF THE THESIS.....	4
1.2 OUTLINE OF THE THESIS.....	5
<b>2 DELETERIOUS PHENOMENA IN PUMP AND FAN SYSTEMS.....</b>	<b>6</b>
2.1 CAVITATION .....	7
2.2 STALL .....	11
2.3 CONTAMINATION.....	11
<b>3 SENSORLESS FLUID SYSTEM MONITORING VIA VSD-BASED PARAMETER ESTIMATES .....</b>	<b>13</b>
3.1 AVAILABLE SENSORLESS MONITORING TECHNOLOGY.....	13
3.2 INTRODUCTION OF SENSORLESS DETECTION METHODS .....	14
3.2.1 Cavitation.....	14
3.2.2 Surge .....	16
3.2.3 Contamination.....	18
3.2.4 Non-return valve operation.....	22
<b>4 IMPLEMENTATION OF REMOTE MONITORING AND SENSORLESS DETECTION METHODS .....</b>	<b>26</b>
4.1 NETA-21 .....	26
4.2 DRIVE COMPOSER PRO .....	30
4.3 MATLAB .....	31
<b>5 SENSORLESS PUMP SYSTEM MONITORING .....</b>	<b>33</b>
5.1 DETECTING CAVITATION.....	35
5.2 DETECTING NRV BREAKDOWN .....	47
<b>6 SENSORLESS FAN SYSTEM MONITORING .....</b>	<b>50</b>
6.1 DETECTING SURGE.....	51

6.2	DETECTING IMPELLER CONTAMINATION .....	56
<b>7</b>	<b>INDUSTRIAL PILOT: DETECTING CAVITATION FROM PUMPS USED IN PAPER MILLING .....</b>	<b>60</b>
<b>8</b>	<b>SUMMARY AND CONCLUSIONS .....</b>	<b>65</b>
8.1	SENSORLESS DETECTION METHODS .....	65
8.2	PILOT EXPERIMENT .....	67
8.3	FINAL THOUGHTS .....	67
	<b>REFERENCES.....</b>	<b>68</b>

## **SYMBOLS AND ABBREVIATIONS**

BEP	Best efficiency point
DCP	Drive composer pro
DDCS	Distributed drives communication system
DTC	Direct torque control
EFEU	Efficient Energy Use
LCC	Life-cycle cost
NPSH	Net positive suction head
NRV	Non-return valve
RMS	Root mean square
VSD	Variable speed drive

$a$	sample index
$b$	sample index
$e$	estimate
$g$	acceleration due gravity
$H$	head
$J$	moment of inertia
$n$	rotational speed
$p$	pressure
$Q$	flow rate
$S$	variable for surge detection
$T$	torque
$t$	time
$\alpha$	angular acceleration
$\rho$	fluid density
$\omega$	angular velocity

# 1 INTRODUCTION

Energy efficiency and environmental values are on the rise in today's world. Partially because of the debated climate change happening around us, emissions are being reduced and regulated more and more with new benchmark goals being set for decades to come. Energy production is shifting from fossil fuels towards renewable energy sources and the overall share of the renewables in total energy production is steadily increasing each year (Lins, 2014). To better utilize our resources, more efficient energy production and usage is necessary. Fluid handling systems have also had their fair share of research on improving energy efficiency. Variable speed drive (VSD) has become a key component to more efficient motor and process control in fluid handling systems, having immense benefits on energy savings when compared to traditional valves with control methods such as throttling or on/off (Al-Khalifah, 2013).

Another ambition driving today's industries, aside from energy efficiency and clean energy, is the Internet of Things. Traditional devices are designed in new ways to get them connected to Internet and their data collected. This allows operation of the devices remotely and grants an access to data that has not been available earlier, at least on such a large scale. Possibilities to create new applications and services are nearly limitless. This requires extensive research and innovation on how we can get the most benefit out of these current technological trends.

Since 2011, Lappeenranta University of Technology has been part of Efficient Energy Use program, EFEU. This program brings together industrial partners and research facilities in Finland to develop new energy efficient solutions for fluid handling systems (CLIC, 2016). This program partly combines the above mentioned phenomena, i.e. creates new ways to improve energy efficiency of a fluid handling system and develops new business opportunities for companies to produce energy efficiency services. This master's thesis continues on the research conducted earlier in the EFEU project, namely on the topic of remote monitoring done by Kimmo Huoman (Huoman, 2015) and VSD-based problem detection methods done by Santeri Pöyhönen (Pöyhönen, 2016). Both of these topics are applied in fluid handling systems, such as centrifugal pumps and fans, to determine whether there are phenomena present that can be deleterious to the system in terms of its efficiency and life time. The following subchapters introduce the objective and contents of this thesis.

## 1.1 Objective of the thesis

The objective of this thesis is to implement and test sensorless VSD-based remote monitoring to detect harmful phenomena in pump and fan systems. Focus is on how the monitoring and phenomena detection can be easily retrofitted to a fluid handling system with an already existing VSD without making changes to the existing system and how the monitoring can be done remotely. External remote monitoring tool is used in combination with VSD to monitor required parameters for the phenomena detection. Effect of data sampling rate is studied to find sufficient rates based on the used hardware's capabilities, the monitored system and detected phenomenon. Sampling rate is also studied from the data logger's point of view. With the equipment used in this thesis, a smaller sampling rate allows for continuous monitoring with the external monitoring unit. Higher rate can be utilized with VSDs own inbuilt data loggers utilizing conditional logging. Unlike the

external logging unit, these inbuilt loggers have restrictions on the amount of stored data due to buffer size. Occurrences of the deleterious phenomena in a fluid system are remotely analyzed from the logged data with Matlab scripts.

## **1.2 Outline of the thesis**

Chapter two introduces pump and fan systems, their life-cycle costs and the deleterious phenomena studied in this thesis. This includes definitions, causes leading to the phenomena and what is the potential damage and the impact on energy efficiency and life-cycle costs of the system. Traditional solutions to detect and prevent these phenomena from occurring are mentioned.

Chapter three discusses the motives of the thesis; what is the need for sensorless system monitoring and what are its benefits when compared to traditional sensors. Already existing, commercially available solutions are presented for the detection of deleterious phenomena and remote monitoring with combined usage of VSD and sensors. Sensorless detection methods that are applied in this thesis are introduced. This includes theory, equations and already done research of the detection methods. Applicability and possible arising problems of these methods are discussed in terms of testing of the sensorless remote monitoring in laboratory environment and its real applications.

Chapter four discusses what is required to achieve sensorless, remote system monitoring. The used hardware is introduced along its data transfer and logging possibilities. Alternative remote data acquisition paths are discussed and the used methods are presented. The software used in data analyzation is introduced as well as general algorithms used to detect the phenomena from measurement data.

Chapter five presents laboratory measurements which are based on the detection methods and the implemented remote monitoring solution. This includes information about equipment used in the laboratory, conducted tests, results gained from the measurements in the laboratory conditions and analysis of the results.

Chapter six introduces an industrial pilot experiment. The implemented methods were used to detect the appearance of one of the phenomena. Results from the sensorless detection method are presented and analyzed.

Chapter seven summarizes the thesis with final conclusions.

## 2 DELETERIOUS PHENOMENA IN PUMP AND FAN SYSTEMS

Electricity consumption in industrialized countries is mostly focused on different applications of electric motors. In the early 2000s, field studies have shown that motors are responsible for 69 % and 38 % of the total electricity consumption of industrial and service sectors. Share of pumps and fans is totaling 38 % of industrial and 40 % of service sector motor end-use (Almeida, 2003). For this reason, energy efficiency and reliability of pump and fan systems is a matter of great importance as the potential for energy savings is large while efficient solutions can be implemented more and more easily. Numerous studies have been conducted about the benefits of variable speed drives on pump and fan systems with varying operation conditions. Controlling flow rates of fluids by reducing the rotational speed of a motor is far more efficient than altering friction in a system through various control valves. Varying speed also allows us to minimize the effects of changing operation point. Even if pump efficiency changes due to a variable rotational speed, the new operation point generally is still more energy efficient than what it would be if the same operation conditions would have been accomplished by throttling.

Life-cycle costs (LCC) of pump and fan systems mostly consist of initial project investments, maintenance costs and energy costs. Distribution of these areas are depicted in Figure 2.1. From these three areas, the energy costs have been estimated to take the largest share in large pumping applications (HI, 2001). Efficiency of a centrifugal pump at the best efficiency point (BEP) is typically 70-80 % (Grundfos, 2009, Forsthofer, 2005 & Evans, 1996). For radial fans, efficiency is up to 75 % (BEE, 2004). The LCC analysis suggests that the best way to reduce the overall system costs is to improve and uphold energy efficiency, for example by controlling the flow rate with a VSD. In terms of maximum efficiency, improvements can be difficult to achieve as it would require upgrading the existing system.

There exists phenomena that reduce energy efficiency of a system while possibly causing mechanical damage along with it thus increasing maintenance costs as well. Preventing, or at least minimizing, the effects of these phenomena improves the lifetime of the system, saves energy and reduces chance of a system failure. When planning to minimize or to prevent these phenomena, the initial investments on the system will become higher than usual but the savings in terms of energy and equipment repair should outweigh the increased investment costs according to the LCC analysis.

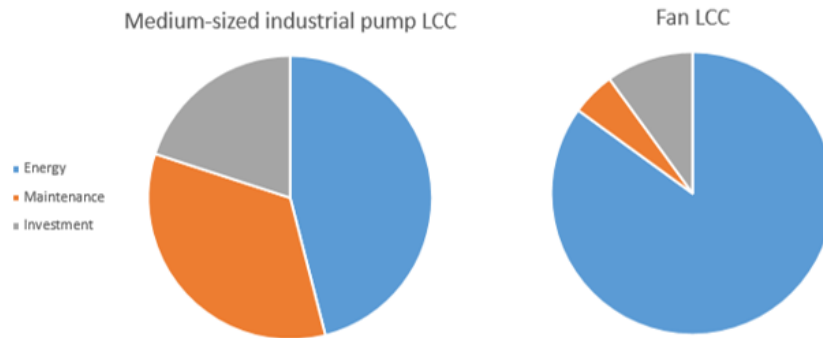


Figure 2.1 A crude LCC analysis of general pump and fan. Energy is the biggest contributor to the overall costs. It is often advisable to focus on improving and maintaining energy efficiency to bring down the total LCC (HI, 2001 & Fläkt Woods, 2015).

Along with speed control, VSDs can bring forth other benefits, namely in terms of pump and fan system monitoring (Orkisz, 2008 & Tamminen, 2013b). External sensors have been traditionally used to monitor fluid systems. This requires additional investments and retrofitting of these sensors is not always practical. VSDs, while also controlling the rotational speed, can also be used as tools for data collection, as they can often provide estimates of the system variables such as torque and rotational speed. This data can be used to monitor the operation conditions of the system, current operation point, power usage, efficiency and to detect phenomena harmful to life cycle of the application (Tamminen, 2013b).

Centrifugal pumps are the most used pump type globally (Grundfos, 2004). Research of the sensorless detection methods referenced in this thesis have been designed and tested with centrifugal pumps in mind. Therefore while all pumps can suffer from detrimental phenomena, focus on this thesis is on centrifugal pumps. Hereafter pumps and pumping systems refer to centrifugal pumps and their fluid systems. This applies to the studied fan systems as well.

## 2.1 Cavitation

One of the most typical deleterious phenomenon affecting pumping systems is cavitation. Cavitation is a phenomenon in which vapor-filled cavities are forming in a liquid and then collapsing later on in a pumping system. The collapses cause damage to the system through mechanical wear and vibrations.

Typically when thinking about vaporization, temperature of the liquid is the first consideration that comes to one's mind. All liquids start to boil and form vapor after their temperature has risen enough, depending on the pressure acting on the liquid. For water, at sea level atmospheric pressure, this temperature limit is 100 °C. In pumping systems, increase of temperature in the liquid can be the cause of the vaporization but more often it is due decreasing pressure of the liquid in the pump. This is why cavitation is in literature sometimes referred to as cavity formation due pressure change, excluding the vaporization

due temperature changes.

Cavitation occurs when the vapor pressure is higher than the pressure acting on the liquid (Forsthoffer, 2005). In centrifugal pumps, there is a pressure drop at the suction side from suction flange to the pump vane inlet, as seen in Figure 2.2. This pressure reduction is a result of friction losses in piping, liquid acceleration and entry shock losses at the vane tips of the impeller (Forsthoffer, 2005). If the pressure drops below liquid's vapor pressure, it starts to evaporate. As vapor bubbles move towards the tip of a pump vane, pressure and velocity of the liquid is increasing. After the liquid pressure has exceeded the vapor pressure, the bubbles implode with adverse effects on the pumping equipment.

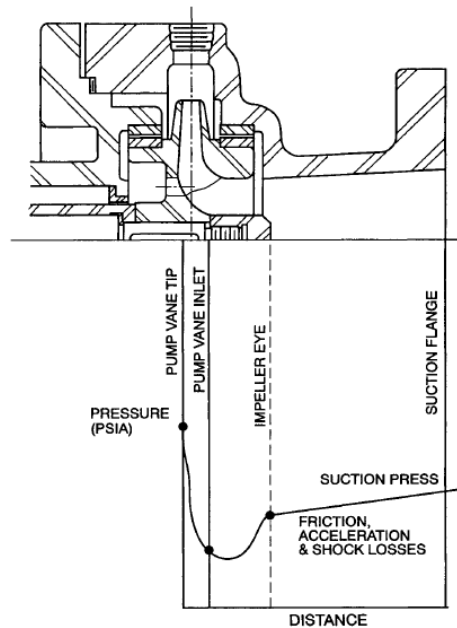


Figure 2.2 Pressure drop in the inlet of a pumping system. The pressure drop from suction flange to pump vane inlet can cause cavitation if there is not enough net suction head available (Forsthoffer, 2005).

This type of cavitation can be prevented by having enough available net positive suction head,  $NPSH_a$ .  $NPSH_a$  is the amount of suction head present at the pump suction above the vapor pressure of the liquid (Volk, 2005). This value consists of the absolute pressure on liquid surface in a suction vessel, a height difference between the liquid surface and a pump impeller's centerline, friction losses at a suction side and the vapor pressure of the liquid in the pumping temperature (Volk, 2005). This value should be estimated as its minimum which means on the lowest possible liquid level in the suction vessel, the highest temperature of the liquid and with the highest friction losses, typically presented when running on maximum capacity. To avoid cavitation,  $NPSH_a$  should exceed the required suction head,  $NPSH_r$ .  $NPSH_r$  depends on the inlet design of the pump and its rotational speed, as seen in Figure 2.3.  $NPSH_r$  curves are typically provided by the pump manufacturer (Karassik, 1976).  $NPSH_r$  is essentially equal to the pressure drop that is shown in figure 2.2. Comparison between  $NPSH_a$  and  $NPSH_r$  should be done at all of the operation points of the pump with worst case scenario typically being at the maximum expected flow (Volk, 2005). However having  $NPSH_a$  greater than  $NPSH_r$  does not completely eliminate the possibility of cavitation occurring in the entire pumping system.

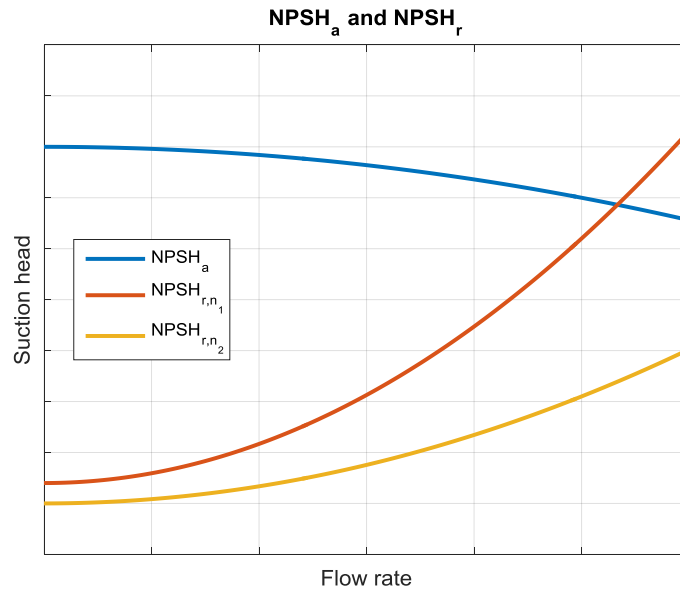


Figure 2.3  $NPSH_a$  and  $NPSH_r$  as function of flow rate. With higher flow rates the available suction head decreases while the required suction head increases. Rotational speed affects the  $NPSH_r$ , as seen on the two  $NPSH_r$  curves. On this figure, rotational speed  $n_1 > n_2$ .

Low flow velocities in an impeller can cause separation of flow stream lines leading to low pressure areas inside the impeller. Depending on the vapor pressure of the liquid this effect can cause cavitation, if the pressure in these low pressure cells is less than that of the liquid's vapor pressure (Forsthoffer, 2005). The impeller vanes' curvature always result in lower velocities at the pressure side of the vanes. Hence vaporization as well as the cavitation damage occur on the pressure side of the vanes. This phenomenon is also known as recirculation (Badr, 2015). Pump's efficiency also drops in the low flow region of a pump curve. This can cause enough increase in the vapor pressure that the liquid vaporizes at the impeller vanes (Forsthoffer, 2005).

Besides suction side, flow recirculation can also occur at the discharge side of a pump. When a pump is run with a high discharge pressure, the pumped liquid can start to circulate inside the housing. As the liquid circulates around the impeller, it must pass through between the impeller and the cutwater of the pump at high velocity. This causes vacuum to develop at the cutwater and hence vaporization of the liquid. The operation point of the pump, where discharge cavitation begins to occur is typically 10 % less than the BEP (Pump World, 2014). This makes pumps controlled by throttling valves more vulnerable to cavitation as throttle control moves the operation point along the pump curve, away from the BEP.

(Brennen, 1994) divides consequences of cavitation into three categories. First there is a material damage as seen in Figure 2.4. Shock waves caused by implosion of the cavitation bubbles cause wear on the material surface, typically in the impeller. Vibrations caused by uneven impeller loading can lead to a mechanical damage in other parts of the system (Volk, 2005). Second effect of cavitation is a reduction of pump performance. A pump will produce less head and flow than its characteristic curve would suggest (Volk, 2005). Third adverse effect of cavitation is a possibility of rotating cavitation and auto-oscillation, which are similar to the phenomena of rotating stall and surge presented in the next

subchapter. They are instabilities in the flow that occur under the cavitation effect and can cause oscillation in the flow rate and pressure (Brennen, 1994).



Figure 2.4 Cavitation damage on propeller. The vane edges are damaged due shock waves caused by imploding bubbles (Wikipedia, 2006).

Cavitation is a costly phenomenon as the damaged parts have to be replaced or they will decrease the overall efficiency and performance of the system, running into a risk of total system failure. In marine industry cavitation damage costs millions each year (Drydock, 2003). In addition to replacing the damaged equipment, valuable production time is also lost as excess time spent on maintenance can directly cut away from production time. The phenomenon is also reoccurring if the operation conditions remain the same so installing new equipment won't solve the problem of cavitation, it just starts the cycle anew.

Avoiding occurrence of cavitation is easier in the design phase of a system. Calculating of the  $NPSH_a$  should be done and the pump sized accordingly or the  $NPSH_a$  to be increased. Typically you want to use the worst case scenario when evaluating the amount of  $NPSH_a$ . In open systems, the  $NPSH_a$  can be increased by lowering the pump or elevating the surface of the surface of the liquid in the suction vessel. In closed systems, the system pressure can be increased. Temperature of the pumped liquid could be lowered to reduce the vapor pressure (Grundfos, 2004). When the operation requires variety of flows, different control schemes should be considered. Throttling may be a cheaper option than installation of a VSD, at least when comparing initial investments, but the damage it can cause to the system through cavitation plus the increased operational costs might be more than enough to justify VSD. Also the LCC of a pump should be kept in mind as the initial investment can be small compared to the other costs during pumps lifetime. The amount of friction in the piping is easier to control while they are being constructed. Diameter of the pipes, length of the piping, the materials used and bends in the system all add up to the friction the pump has to overcome which increases  $NPSH_r$ . After the installation is complete reduction of cavitation damage can be much more difficult and expensive (HI, 2004 & Karassik, 1976).

## 2.2 Stall

Stall is a phenomenon that occurs when there is insufficient amount of air moving across the fan blades and the flow detaches from the blades (Tamminen, 2013b). This separation often carries over to the following blades, leading to a cascading effect (US EERE, 2003). This results in a pressure drop (Figure 2.5) as well as pressure oscillation in the fan output (Tamminen 2012). Insufficient flow typically means that we are moving away from the BEP of the fan by inefficient control methods like throttling valves or the fan has been oversized for its purpose. If the stall is occurring on all of the fan blades, the fan system is surging which could lead to a complete flow reversal.

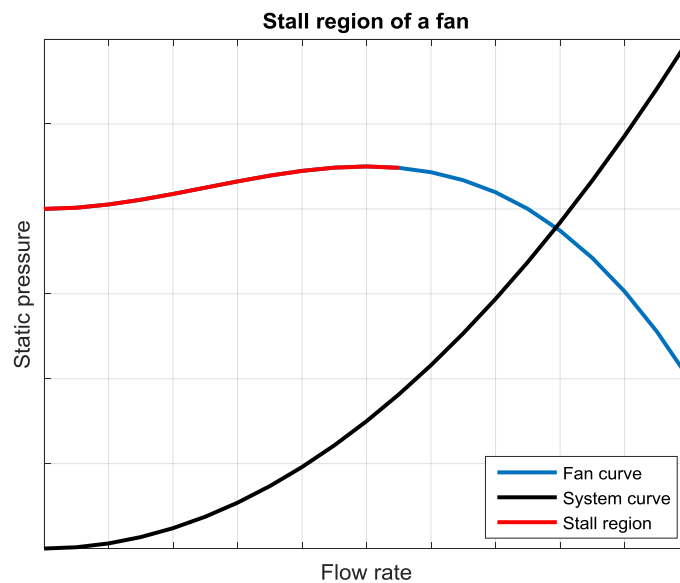


Figure 2.5 Stall region of a centrifugal fan. Operation point should not be in the stall region as it leads to pressure drop, lower efficiency and system vibrations.

Occurrence of stall depends on the type of the fan being used. Axial fans in particular are vulnerable to stall and should not be used in systems with varying flow requirements. Radial fans do not suffer from stall as much as they operate without relying air slipping across the blade surfaces (US EERE, 2003).

Stall has similar effects to the system as recirculation. Usually there is a severe increase in fan noise (Aerovent, 2012), vibrations in the fan and mechanical stress in the system (Tamminen, 2013b). This can cause mechanical damage to the bearings, the shaft or the impeller. Efficiency of the fan system is also less than optimal. This leads back to the system design and possible oversizing of the fan for its designed purpose. A smaller fan would be more efficient, while also costing less in terms of initial investment and using less energy (Aerovent, 2012).

## 2.3 Contamination

While fluid travels through a fan system it can contain contaminants in it. These contaminants can stick to surfaces of a fan system such as piping and impeller, increasing the friction that the motor has to overcome. Contamination buildup on the impeller will eventually lead to a less efficient system as total mass of the impeller increases. In

pumping systems contaminants can clog up the piping or the impeller causing a total system failure.

The contamination of a fan impeller could be considered as a common cause of a failure in fan systems (Tamminen, 2013a). Careless maintenance can cause a mechanical imbalance on the fan impeller as mass gets unevenly distributed on the impeller surface. As time goes on this can cause failure of the fan system. Depending on the application, the damage caused by a fan system failure could be extensive. In cooling systems it can lead to overheating and breaking of other system components. Downtime caused by fixing the fan system leads to loss of production and unnecessary interruption to the production, for example in power plants (Tamminen, 2013a).

Visual inspection has been the traditional method of noticing contamination buildup on a fan impeller. However visual inspections require skilled personnel, it can be time consuming and it might not always be possible. It is much more practical to have other means of noticing contamination for fans in remote locations. Sensors can be used to notice increasing vibrations in the system but they increase the complexity of the system. Sensors add another part that requires initial investments, maintenance and repair. Retrofitting the sensors can also be impractical.

While avoiding contamination buildup can be impossible in some fan systems, monitoring of the contamination buildup at least provides us with information when the impeller should be cleaned. This can help us schedule equipment maintenance more efficiently minimizing excessive inspection of the impeller condition and cleaning routines.

### **3 SENSORLESS FLUID SYSTEM MONITORING VIA VSD-BASED PARAMETER ESTIMATES**

Traditional system monitoring relies on external sensors to provide data about some physical phenomenon or quality (pressure, temperature, rotational speed, torque, height, weight, etc.). Modern technology allows implementation of sensorless monitoring methods that are based on parameter estimates rather than actual measurements.

Obvious benefit of sensorless monitoring methods is that traditional sensors aren't required. Sensors bring in additional costs as investment, installation, maintenance, repair and calibration are all necessary costs for sensors (Wilson, 2005). Of course sensorless parameter estimation has its own drawbacks. The estimates are based on models and are less accurate than direct measurements. While sensors are not used additional hardware is still required to provide the estimates. In fluid handling systems VSDs can be used to provide necessary sensorless monitoring. The available monitored variables are limited but practically every commercial VSD provides torque and rotational speed estimates (Holtz, 2000).

#### **3.1 Available sensorless monitoring technology**

There already exists a market of sensorless control and monitoring for pumps and fans. Manufacturers are providing integrated solutions with pump and VSD combined as well as automated control and operation during fault conditions.

- Emotron M20 (Emotron, 2016) is a sensorless load monitor which can be used for pump and fan applications to detect over- or underload.
- PumpSmart PS20 (ITT, 2016) is a similar load monitor which doesn't require additional sensors.
- PumpSmart PS200 is a VSD that can monitor flow rate without additional sensors by modeling the pump's power curve (Xylem, 2016). When looking at the phenomena presented in this thesis, PS200 also includes cavitation control. It is done by monitoring suction conditions and when the  $NPSH_a$  drops, the rotational speed of the pump is automatically reduced to lower the  $NPSH_r$ .
- Taco Inc. offers pumps with integrated speed drives for sensorless control (Taco, 2013). Characteristic curves are pre-embedded in the controller memory during manufacturing phase. With power and speed monitoring the system can identify head and flow rates for control without feedback from external sensors.
- Grundfos e-pump series offers a wide range of integrated solutions where a pump, a motor and a VSD are integrated to a single unit (Grundfos, 2016). While external sensors can also be added, there is default built-in monitoring of various parameters such as power consumption, energy consumption and amount of head.

Available condition monitoring is focused on flow rate, power consumption, produced head and energy consumption while adjusting rotational speed when necessary. While useful on their own, these parameters can also be utilized for detecting harmful phenomena in a fluid handling system.

## 3.2 Introduction of sensorless detection methods

Overall if the already beneficial equipment for process control (VSD) can be utilized for data collecting, the required condition monitoring can be done with zero additional investments in sensor equipment thus gaining more value out of the installed VSD. When condition monitoring requires only estimates that the VSD can provide, sensorless condition monitoring of a system can be implemented. However not all of the variables in a system can be estimated by VSD and sensors still have their place in such cases.

The sensorless detection methods for the phenomena introduced in chapter two are presented in this subsection. Methods for fan systems monitoring were part of doctoral thesis of Jussi Tamminen (Tamminen, 2013b) and the cavitation detection was part of doctoral thesis of Tero Ahonen (Ahonen, 2011b). Condition monitoring of a non-return valve was presented in (Ahonen, 2015).

### 3.2.1 Cavitation

A novel method for sensorless cavitation detection with a VSD is presented in (Ahonen, 2011a). The detection method is based on behaviour of rotational speed and shaft torque in a pumping system. Estimates for these variables can be provided by a VSD. Following are the hypotheses of the presented method:

- Occurrence of cavitation in a centrifugal pump results in vapor that may obstruct the fluid flow, especially in the case of fully developed cavitation affecting the performance of the pump. This will lead to an intermittent flow rate which increases the amount of time-domain variation in power consumption.
- Variation of the power consumption can be detected with a VSD by monitoring estimates of rotational speed and shaft torque ( $n$  and  $T$ ). While a pump is operating in a steady state, as in the reference value of the rotational speed and characteristics of the process stay constant, an increased time-domain variation of rotational speed or shaft torque estimate when compared with a magnitude of variation in normal conditions is a symptom of cavitation.
- Depending on the system and the applied control method of the VSD, occurrence of cavitation can affect either the rotational speed or the shaft torque estimates or both of them.
- Depending on the characteristics of the pump and the process, estimates of the rotational speed and the shaft torque should be monitored for several seconds to detect intermittent operation of a centrifugal pump.
- The time-domain variations of the rotational speed and shaft torque estimates can be quantified by calculating root mean square (RMS) values of the alternating components in the estimates.

In short, we can compare the magnitude of variation in rotational speed and shaft torque estimates with reference values gained from known steady state where cavitation does not occur. Increase in the time-domain variation is a sign of cavitation.

RMS values of the variations of rotational speed and shaft torque,  $n_{rms}$  and  $T_{rms}$ , are calculated from the following equations for discrete-time estimates  $x(n)$  as follows:

$$x_{DC}(n) = \frac{1}{M} \sum_{k=0}^{M-1} x(n-k), \quad (1)$$

$$x_{AC}(n) = x(n) - x_{DC}(n), \quad (2)$$

$$x_{RMS}(n) = \sqrt{\frac{1}{M} \sum_{k=0}^{M-1} x_{AC}^2(n-k)}, \quad (3)$$

where  $n$  and  $k$  are discrete-time indices,  $M$  is the number of collected samples and subscripts <sub>DC</sub> and <sub>AC</sub> denote direct and alternating component of an estimate. The direct component is basically a mean value of the samples and alternating component is deviation from the mean value for each sample.

To determine whether or not the RMS values have increased, normal RMS values  $n_{rms}$  and  $T_{rms}$  of a centrifugal pump should be determined for reference when the pump is running absent cavitation. These values are system specific. The normal values could be obtained automatically during regular operation or with a separate identification run. After the normal values are known we can continuously calculate  $n_{rms}$  and  $T_{rms}$  and compare them with the normal values. If the ratio between current and reference values rises above a certain threshold, cavitation has likely occurred. There is no universal threshold value for all pumping system, but the reference study suggests that the ratio should be at least 1.5-2.0 for both of the parameters.

The method is prone to error if there is change in process control while the reference values stay constant. This could result in erroneous cavitation warning or cavitation might occur unnoticed. The method has been tested in steady state operation of the pump for these reasons but this could be an area for future improvements, as to include the effect of rotational speed and process changes on the reference estimates.

Laboratory measurements were presented to test the detection method in (Ahonen, 2011a). The used pumping system consisted of a Sulzer APP 22-80 centrifugal pump, an ABB 11 kW induction motor and an ABB ACS800 VSD. Cavitation conditions were formed by driving the pump at a 140 % relative flow rate, increasing the rotational speed and increasing the friction losses in the system at the suction side with control valves. These actions together significantly reduced the ratio between  $NPSH_a$  and  $NPSH_r$ . In this test case, cavitation should clearly occur as the ratio between the available and required NPSH drops below 1.35. This limit is based on the pump's inlet velocity. For medium and low energy impellers, which account for more than 90 % of applications, the  $NPSH_a$  should be 35 to 50 % higher than  $NPSH_r$  to avoid cavitation and develop essentially rated total head (Karassik, 1998). Incipient cavitation typically occurs with higher NPSH ratios (Schiavello, 2009) and its reliable detection requires visual or acoustic measurements. This is why incipient cavitation was left out of the evaluation of the detection method. Results from the measurements show that the decreasing NPSH ratio is directly linked to the increasing ratio of RMS estimates as seen in figure 3.1.

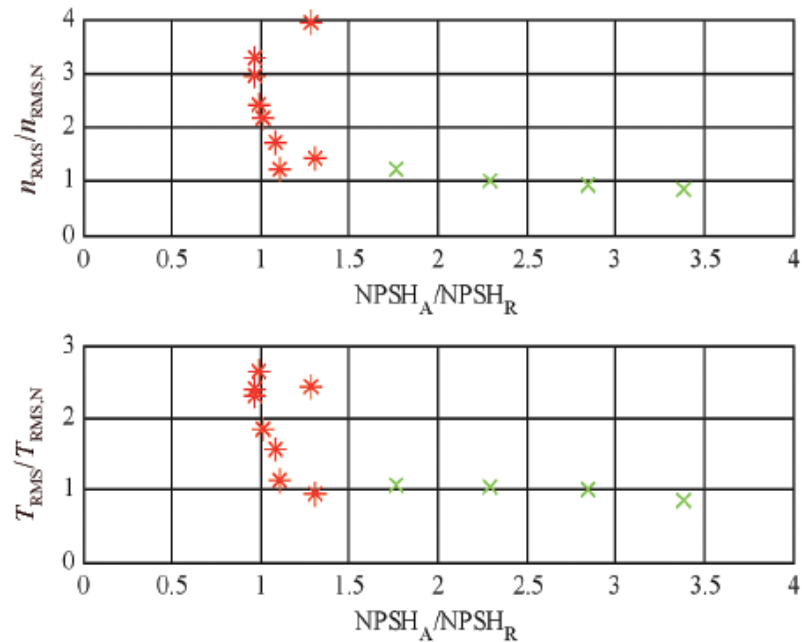


Figure 3.1 Testing of the cavitation detection method (Ahonen, 2011a). RMS ratios of torque and speed variation as a function of NPSH ratio. Occurrence of cavitation increases the  $n_{RMS}$  and  $T_{RMS}$ .

As the  $NPSH_a$  draws closer to the  $NPSH_r$ , the amount of variation in measured torque and rotational speed starts to increase and ultimately the threshold ratio is reached. Operating the pump in a region where the available and required NPSH are nearly equal, cavitation can be detected clearly. The estimated values were verified with measurements from Dataflex 22/100 speed and torque measurement shaft. The measured values showed similar characteristics as the estimates when the pump was prone to cavitation.

To use this method efficiently in this thesis, it is crucial to get correct reference values. In laboratory measurements this can be easily done with a test run. In industrial applications such test runs might not be feasible. Probable solution is to get the reference values during normal operation when there is no cavitation noise present or when the pump is known to run at its BEP or at least near in its proximity. Another approach would be to develop an equation for the reference values based on system variables. However such would require testing with multiple pumps and motors to get accurate references and minimizing erroneous cavitation detection. In this thesis the approach to get the reference values is to analyze normal operation for each system individually and to determine suitable reference values from there. Estimation of torque and rotational speed variation in normal operation conditions based on system variables could be a subject of a further study if deemed useful enough but it is out of the scope of this thesis. Additionally, a sufficient sampling rate for cavitation detection has to be determined. In (Ahonen, 2011a) the phenomenon is shown to affect low frequency components (0-10 Hz) of torque and speed estimates. As such the sufficient sampling frequency is unlikely to be high either.

### 3.2.2 Surge

(Tamminen, 2012) presents method for sensorless surge detection through a VSD. The detection method is based on low frequency fluctuation in the required shaft power. The fluctuation can be observed through torque and rotational speed estimates of the VSD. A

fan has to be operated at a constant torque or rotational speed reference during measurements. RMS values for the low frequency fluctuations are calculated from the torque and rotational speed estimates without the DC level. This estimate is called unbiased estimate  $e_{unbias}$  and it can be calculated as

$$e_{unbias} = e(t) - \bar{e}, \quad (4)$$

where  $e(t)$  is a parameter estimate at time instance  $t$  and  $\bar{e}$  is a mean value of the estimates. The unbiased estimates are filtered with a digital low pass filter so that only the low frequency fluctuation is present. Decimation of the signal could also be used for this. The frequency band in the study was from 0 to 2 Hz. The final RMS value can be then calculated from the filtered, unbiased estimates  $e_{filtered}$  as

$$e_{RMS} = \sqrt{\frac{1}{m} \sum_{n=0}^{m-1} e_{filtered}^2(n)}, \quad (5)$$

where  $m$  is the total number of samples and  $n$  is the index of a sample. Obtained RMS values from equation (5) are used for surge indication. The fluctuation values for the torque and rotational speed are combined to ensure more reliable detection as the proportion in which the fluctuation is visible is related to the control loop of the VSD and the parameters of a built-in PID controller. Additionally the absolute RMS values of the fluctuation are on a different scale as 1 rpm is not equal to 1 Nm.

When a fan system is operating away from its surge region, current RMS values can be used as the reference point for normal variation. Using the reference values, dimensionless number can be calculated for surge detection. This nullifies the effects of the inequality between rotational speed and torque. A dimensionless number  $S$  acts as an indicator for the current fan operation and can be calculated from the current and reference RMS values as

$$S = \sqrt{\left(\frac{n_{RMS}}{n_{ref}}\right)^2 + \left(\frac{T_{RMS}}{T_{ref}}\right)^2}. \quad (6)$$

Surge in a fan system is detected if  $S$  exceeds a certain limit. In (Tamminen, 2012) this limit was selected to be 2. With no further information available, this is the baseline adopted in this thesis as well. In case of inaccuracies, this limit can be changed later to better represent the current system as it is not a universal value.

Aside from filtering the samples and later on combining the calculated RMS values to a one dimensionless number, this method utilizes same principles as the previously introduced cavitation detection. As such the difference in actual sensorless monitoring implementation might be that a pump is replaced by a fan.

The surge detection method was tested in (Tamminen, 2012) in laboratory environment and the results were compared with another detection method that was based on a reduced dispersion of the output pressure. Testing equipment consisted of a Fläkt Woods Axipal BZI 630 VA axial fan, an 11 kW ABB induction motor and an ABB ACS850 VSD. The measurements included three different rotational speeds. With each speed a control valve was set from open to close with discrete valve settings. At each operation point, the torque

and rotational speed values were sampled and RMS values were calculated. From the RMS values, surge indicator  $S$  was calculated with (6). Results of the tests are shown in figure 3.2. At high rotational speeds, there are erroneous detections of the surge. In general same results were gained with the proposed method and the reduced dispersion method.

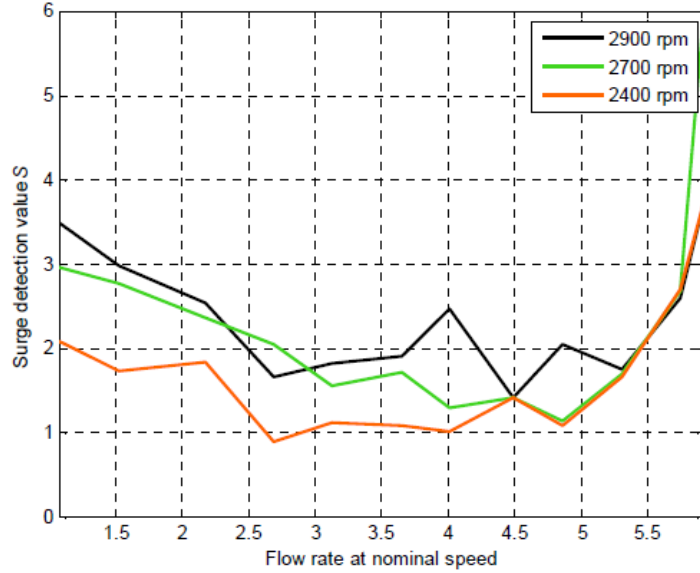


Figure 3.2 Results of surge detection method testing. When the fan moves away from the operation point, surge can be detected (Tamminen, 2012). Increased rotational speed provided false surge detection if the threshold for surge detection remains at constant.

For the purpose of this thesis, the method presented in (Tamminen, 2012) provides surge detection accurately enough. Increasing the predetermined limit of  $S$  indicator can eliminate inaccuracies with higher rotational speeds.

Sampling of the torque and rotational speed estimates was done in (Tamminen, 2012) at 500 Hz frequency for duration of 6.4 seconds. Therefore continuous sampling is not necessary and the required samples can be taken during a short time period. It may be possible to use same sampling frequency and time when detecting presence of cavitation in a pumping systems and surging in a fan system as they both utilize torque and rotational speed estimates during a steady state operation.

### 3.2.3 Contamination

A method for contamination detection is presented in (Tamminen, 2013a). It is based on mass increase of a fan impeller. As contamination builds-up, fan moment of inertia increases steadily. Contamination can be detected if the current fan moment of inertia can be monitored.

Torque  $T$ , moment of inertia  $J$  and angular velocity  $\omega$  are connected as shown in equation (7)

$$T = J \frac{d\omega}{dt} = J\alpha, \quad (7)$$

where  $\alpha$  is angular acceleration. A change in fan moment of inertia can be determined

from the ratio between torque and angular acceleration. When torque change is a stepped constant torque, the angular velocity can be written as a function of time

$$\omega(t) = \alpha t + \omega_0 = \frac{T}{J}t + \omega_0, \quad (8)$$

where  $t$  is elapsed time and  $\omega_0$  is the initial angular velocity. From equations (7) and (8) it can be seen that angular acceleration remains constant in time domain and is solely dependent on applied torque and the moment of inertia. If the torque reference remains constant, angular acceleration is solely a function of the moment of inertia. In a fan system, the moment of inertia is a sum of motor inertia, initial moment of inertia of a clean impeller and the moment of inertia caused by contamination buildup in the fan. This applies when the transfer of fluid is not taken into account. The total moment of inertia of the fan system is presented in (9).

$$J_{Fan} = J_{Motor} + J_{Impeller} + J_{Contamination} \quad (9)$$

When the measurements for reference and current values of  $\alpha$  and  $T$  has been made, the change in moment of inertia can be calculated as

$$\Delta J_{Fan} = \frac{T_2}{\alpha_2} - \frac{T_1}{\alpha_1}, \quad (10)$$

where  $T_2$  and  $T_1$  are torque steps used for measurement of  $\alpha_1$  and  $\alpha_2$ . When the fluid being transferred is taken into account, the linear angular velocity increase is detectable only when the torque required to increase rotational speed of the fan is dominated by the fan moment of inertia. At higher speeds, the torque requirement is dominated by the transferred fluid and the angular acceleration decreases although no change has happened in fan moment of inertia. As a result, the detection of the contamination with higher speeds is much more difficult.

(Tamminen, 2013a) introduces methods for determining the appropriate rotational speed region where the angular acceleration remains constant and the torque requirement caused by transferring of the fluid is minimal. The torque requirement of a fan in a static state is calculated with

$$T = \left(\frac{n}{n_0}\right)^2 T_0, \quad (11)$$

where torque and rotational speed relation of a single case is known, for example nominal torque-speed pair. From the current rotational speed  $n$ , the torque requirement  $T$  is known. From (11), the following equation can be derived for torque ratio, which represents how much of the required torque is caused by the moment of inertia

$$R_T = 1 - \left(\frac{n}{n_0}\right)^2. \quad (12)$$

Now  $n_0$  is the final rotational speed of the fan. Selecting  $R_T$  as 0.95 (95 % of the torque requirement is caused by fan moment of inertia), the upper rotational speed limit can be calculated by solving  $n$  from equation (12). Since estimates for the rotational speed at low

speeds can be erroneous, lower limit for the speed should be selected. (Tamminen, 2013a) uses 3 % of the motor synchronous speed but states that this is entirely arbitrary. With the upper and the lower speed limit, a change in impeller mass and contamination can be detected from between the limits during fan startup when using torque step as control reference. Figure 3.3 illustrates the behaviour of rotational speed as a function of time and torque with the linear trend line plotted on the calculated limits.

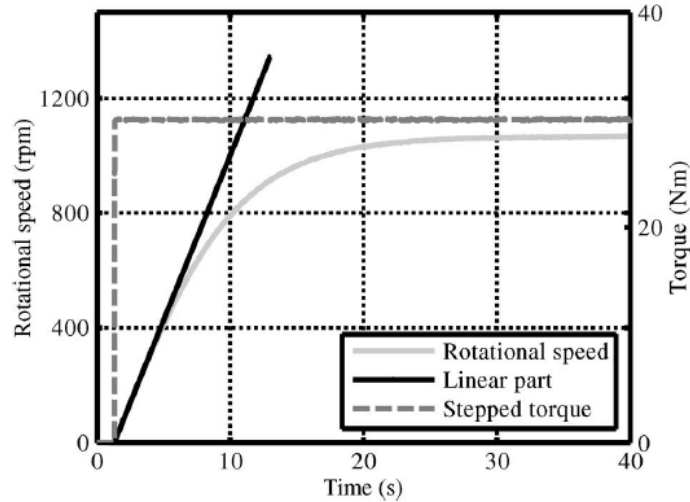


Figure 3.3 Rotational speed of a fan as function of time with torque step applied. The linear part is a region between calculated upper and lower speed limits where the torque requirement is dominated by moment of inertia while transfer of the fluid has minimal effect (Tamminen, 2013a).

As the amount of contaminants on the fan impeller builds-up, slope of the linear part decreases as does the angular acceleration. Tests carried out by (Tamminen, 2013a) to verify this method consisted of laboratory measurements on Fläkt Woods Centripal EU 4 MD 630 radial blower, an ABB induction motor and an ABB ACSM1 VSD that uses direct torque control, DTC. The increasing mass due contamination was simulated by fastening bolts symmetrically to the fan impeller. In real applications the mass buildup on the impeller surface is not symmetrical and the contaminants can affect the mechanical balance of the fan which makes noticing excess mass crucial. With different torque references, results were promising and the detection method was verified as seen in Figure 3.4.

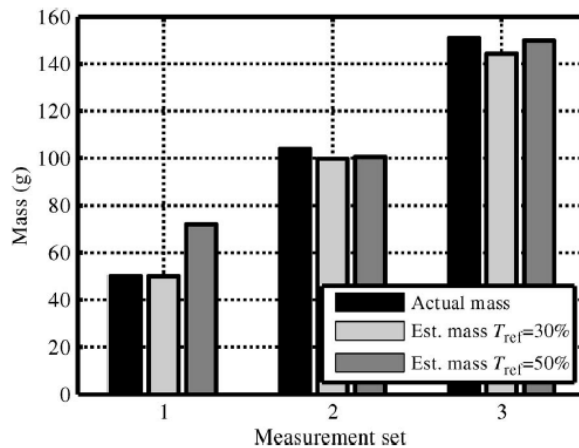


Figure 3.4 The results from the laboratory tests of fan impeller mass detection method. Aside from 50 % torque reference on measurement set 1, the method seems to produce accurate estimates

of the excess mass on the fan impeller (Tamminen, 2013a).

However traditional fan systems are not operated with torque control, rather their rotational speed is being controlled. As such the method presented in (Tamminen, 2013a) can't be directly applied to most of the fan systems with a VSD. Figure 3.5 shows an example of torque behaviour during a fan startup with speed control. The torque is not constant as compared to figure 3.3.

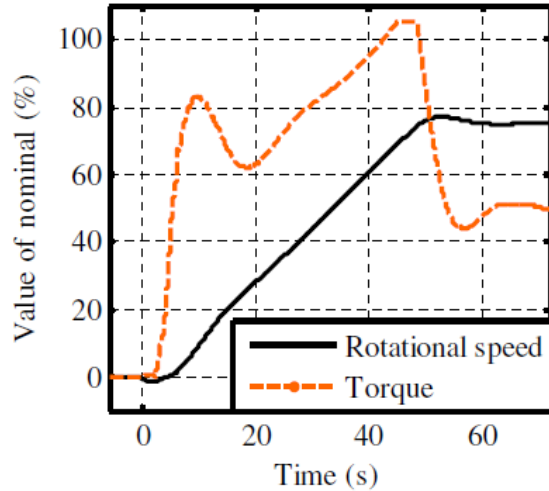


Figure 3.5 Fan startup with rotational speed control. The torque is not constant as it would be with torque control (Tamminen, 2015).

(Tamminen, 2015) provides two methods for detecting contamination when speed control is used in fan systems. First is the integrated torque method where the inertia of fan can be calculated from equation

$$J = \frac{\int_{T_1}^{T_2} T(t) dt}{\omega_2 - \omega_1}, \quad (13)$$

where the torque is between time instances where the angular velocities are  $\omega_2$  and  $\omega_1$ . If the torque is constant such as in the first and second peak as seen in Figure 3.5, the equation (13) can be written as

$$J = \frac{T}{\Delta\omega}, \quad (14)$$

where  $T$  is a constant torque and  $\Delta\omega$  is a difference in rotational speed. This method is referred as the first peak method and it is a special case of the integrated torque method. These two methods were tested in a case study in (Tamminen, 2015). The case involved 7000 hours of torque and rotational speed data from a centrifugal fan that was being used to transfer heat gases. Results from the case study showed that the methods were applicable. Both of the methods showed noticeable increase in fan moment of inertia over time with a significant drop in the moment of inertia after the fan was cleaned. The first peak method proved to be more accurate than the integration method with coefficient of correlation of 0.76, compared that to the 0.25 of the integrated torque.

From the presented contamination detection methods, the integrated torque method seems to be the most usable. As most of the fan systems operate with speed control rather than

torque control, the integrated torque method and the first peak method are more applicable in real applications. From these two detection method, the first peak has been proven to be more accurate in an industrial case study, but it is a special case of the integrated torque method which may render it unusable in certain fan systems.

The data acquisition during the fan startup has to be done with a sufficient sampling frequency and duration. This is entirely application dependent as the startup time can vary from seconds to minutes. Determining suitable parameters is important as the in-build data logging possibilities of a VSD can be very limited in terms of sampling frequency and data buffer size. Commercial, external data monitoring units can provide more flexibility in these areas but they might require additional measurement equipment.

### 3.2.4 Non-return valve operation

In terms of equipment malfunctions, one way a VSD can be used is to monitor the condition of a non-return valve. Non-return valves (NRVs) are used in fluid systems to prevent a flow in one direction while allowing it in the other direction. In industry, NRVs could be used at wastewater stations in pumping applications or storing pressurized gas to a pressure vessel in a compressor system. When properly working these valves prevent all of the possible return flow and as such are a critical part of fluid handling systems to ensure safe and reliable operation.

Sensorless condition monitoring of a NRV was studied in (Ahonen, 2015). The study proposes two methods that are based on the shutdown behaviour of the system. When the NRV is working properly, there is no need to compensate reversed impeller rotation due to the return flow as it is prevented by the valve. The shutdown behaviour can be monitored with variable estimates of a VSD. A normal shutdown behaviour with a speed ramp and a working NRV is presented below in Figure 3.6.

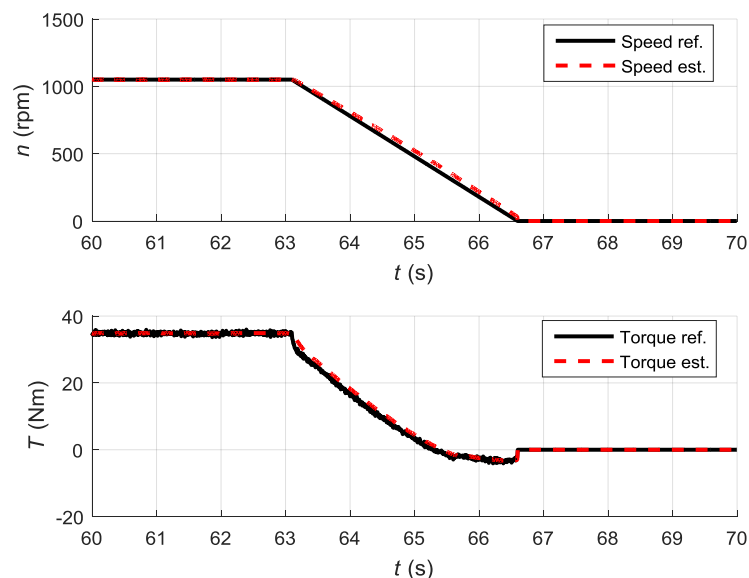


Figure 3.6 Normal shutdown behaviour of the pumping system with working NRV. The system is shutdown with a speed ramp. There is no need to compensate for the reversed impeller rotation as there is no return flow.

After a NRV has been damaged, the motor will have to provide torque to compensate for

the reversed impeller rotation as there exists some amount of return flow depending on the severity of the leakage. The first proposed method is utilized when a pumping system is shutdown with a decelerating rotational speed ramp. Torque can be monitored during the shutdown as long as the VSD is modulating and providing parameter estimates. Figure 3.7 shows the shutdown behaviour with a broken NRV. The NRV breakdown has been simulated by removing it from the piping.

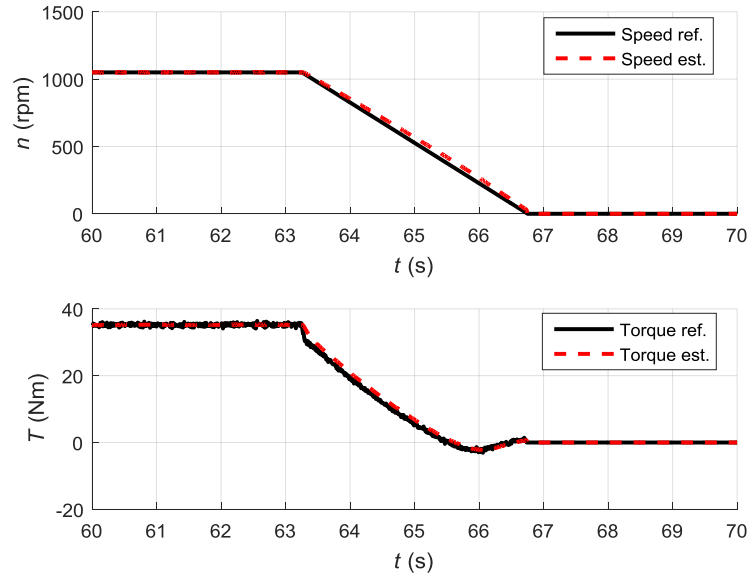


Figure 3.7 Shutdown behaviour of a pumping system with a broken NRV. Excess torque has to be provided for the desired shutdown behaviour. Parameter values in the figure are provided by a VSD. In this case NRV has broken down completely and there is maximum amount of return flow.

Failure of a NRV can be detected from the shaft torque as seen in Figure 3.7. Behaviour of the shaft torque during a normal shutdown operation with a working NRV (Figure 3.6) can be stored as a reference behaviour as the proposed method assumes that the shutdown behaviour remains constant when the NRV is operating correctly. The reference is stored as  $T_{est,ref}(n_{est})$  where  $n_{est}$  goes from  $n_{ref,start}$  to 0 rpm. The  $n_{ref,start}$  refers to the rotational speed from which point onwards the shutdown behaviour of the torque will be monitored. This starting point depends on the NRV in use, as the reference value should be above the threshold where the NRV normally closes down. After the reference behaviour has been identified, the following system shutdowns can be monitored to find out if the instantaneous torque behaviour changes and more torque is required to realize the desired stop ramp. If this happens to be the case then the NRV is not working properly and maintenance may be required. (Ahonen, 2015) provides a method for realizing the comparison between shutdown behaviours. A cumulative torque sum can be calculated from the reference behaviour,  $\sum T_{est,ref}$ , and the following measurements,  $\sum T_{est}$ . Ratio between these two sums can be calculated, and if a predefined ratio limit has been reached then the NRV breakdown can be detected.

Some problems with this method are presented, as the shutdown behaviour is affected by system characteristics, NRV characteristics and the amount of return flow. Difference between the torque sums  $\sum T_{est,ref}$  and  $\sum T_{est}$  in a case of an opened NRV can vary between each shutdown instance. Additionally the rotational speed range can limit the

amount of samples we can get from the torque estimate and hence affect the accuracy of the results. Also the method is unable to detect NRV failure with a stopped pump. (Ahonen, 2015) suggests modifications to the shutdown operation to eliminate these issues. The shutdown operation could be modified so that the VSD can estimate the pump operation when there is zero rotational speed and is also able to prevent reverse rotation of the pump (Figure 3.8). This is achieved in torque control mode instead of using rotational speed control. The pump shutdown operation would now be initiated with a zero torque reference. This is the second monitoring method. Results from the second method with a broken NRV are presented in Figure 3.9.

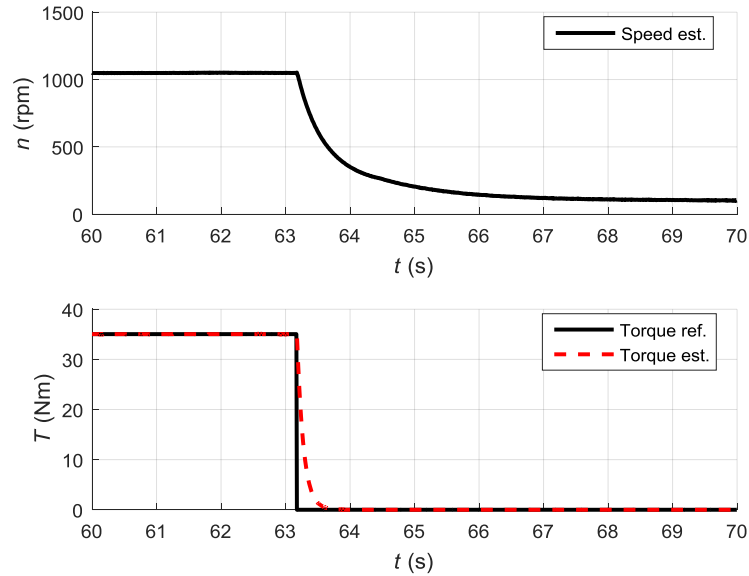


Figure 3.8 Normal shutdown operation with a working NRV. The system is shutdown with a zero torque reference. As the NRV is working as intended there is no need to provide excess torque resulting in smooth torque curve during system shutdown.

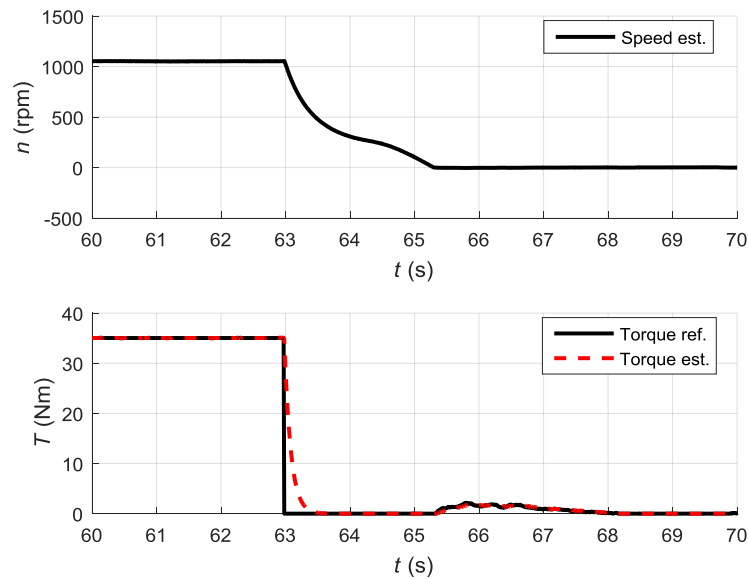


Figure 3.9 Torque controlled shutdown with a broken NRV. Additional torque has to be provided for the desired shutdown behaviour. Parameter values in the figure are provided by a VSD. The NRV does not provide any deterrent to return flow and has been broken down completely.

The results from the first method (Figure 3.7) verified the assumption that a fault in a NRV can be detected by comparing the reference shutdown and following shutdown behaviours of the shaft torque estimate. In the conducted tests the difference between the torque sums was clear but it was stated that it may be difficult to determine a threshold value for the sum ratio which would indicate a faulty NRV. The results from the second method (Figure 3.9) showed that a NRV malfunction can be detected more clearly with a torque controlled shutdown as there is a need to provide excess torque to prevent the reversal of impeller rotation. While the second method could be better as it does not require any knowledge about the correct shutdown behaviour and less computations are needed, the second method requires use of a torque control mode which in practice can limit the usability of this method as we can't always change shutdown operation at will. In practice, the end user might not want any alterations done to the VSD, its parameters and control mode. As such only one of the methods might be usable and in the case of more often used speed control, it is the first method.

## **4 IMPLEMENTATION OF REMOTE MONITORING AND SENSORLESS DETECTION METHODS**

Basis of the phenomena detection in this thesis is that the system monitoring is done remotely without sensors and the required hardware can be easily retrofitted to an existing fluid handling system. Different approaches can be taken for implementing remote monitoring, as there are variety of VSDs and data loggers available on the market each with their own properties, possibilities, programs and limitations. In the future, the remote monitoring application could be a real-time software, where the VSD does the required calculations based on the monitored parameter estimates and provides the required key variables that denote the occurrence of harmful phenomena. Alternatively the VSD could forward the required parameters through a fieldbus and the data could be processed afterwards with whatever suitable program. Monitoring of the system through cloud service has been studied (Huoman, 2015) as it allows practically limitless processing power and data storing capabilities. These would probably be the most elegant solutions, as the only required additional component in a fluid handling system would be a suitable VSD which one could argue is already necessary. However this requires that the VSD is programmable with enough build-in functionality to make it not only possible to provide parameter estimates, but also sample, store, use and transfer them sufficiently. As of now, VSDs are more or less used solely as control units for motors. They can already contain some built-in data logging functionality, for example ABB and Eaton already provide VSDs with device integrated data logger functionality (ABB, 2013 & Eaton, 2016).

For this thesis it is required that the used VSDs can provide estimates for torque and rotational speed, as these variables are used in all of the detection methods presented in the chapter three. This matter is very much a nonissue as these parameters estimates are available practically in every VSD (Holtz, 2000). Since data storing capabilities of VSDs are currently limited, the VSDs should be able to connect to an external data logging device, which stores the provided parameter estimates. Of course possible built-in data logging capabilities could be used if it's practical. The data logger unit should be compatible with multiple different VSDs, in terms of number of units connected to it and different VSD models. Used sampling frequency should be adjustable and there has to be enough memory for the collected data. Additional requirement for possible further development would be an option to transfer the collected data to a cloud service (Huoman, 2015). This could be a feature either in the VSD or in the data logger.

### **4.1 NETA-21**

Core component of the implemented sensorless remote monitoring solution was ABB NETA-21. It is a remote monitoring tool which allows monitoring and adjusting of several ABB frequency drives via Ethernet as well as logging of their parameters (ABB, 2013). It is compatible with a number of different ABB frequency drives and can be retrofitted to existing system easily enough. The network connection of the NETA-21 can be established with either direct cable connection to a system network or via 3G USB modem. The USB modem might become particularly useful in remote locations where direct cable connection is not feasible. Simplified data flow from VSD through NETA-21 to a PC is presented in figure 4.1. This figure shows the basic data flow utilized in this thesis. In (Huoman, 2015) cloud based remote monitoring was realized where there is no direct interaction between end-user and the remote monitoring tool.



Figure 4.1 Simplified data flow diagram. The VSD is controlling the motor while NETA-21 monitors and logs the desired variables from the VSD. The data logged by NETA-21 unit is stored and later accessed with a PC for further analysis.

Depending of the drive or drives in use, communication with NETA-21 can be realized with various different connection types. Supported protocols include drive panel bus over EIA-485, Ethernet PC tool communication, Modbus/RTU via RS-485 and with additional NEXA-21 extension unit, logging can be done via distributed drives communication system (DDCS) by utilizing fiber optic cables. Up to 32 devices can be connected with panel bus, Ethernet or Modbus/RTU and up to 10 devices with fiber optics using ring topology (ABB, 2014).

The data collected by NETA-21 is stored to a SD/SDHC card. The memory card is accessible through web UI of NETA-21. Standard SD card offers storage capacity up to 2 GB and SDHC up to 32 GB (SDA, 2016). The available memory should practically always be sufficient but it is dependent on sampling rates, duration of data logging intervals, the number of sampled parameters and frequency of logging intervals. In the case of requirements of the detection methods presented in this thesis, two monitored parameters should be enough and the logging does not have to be continuous, as only monitoring of the startup and steady state operation when cavitation and surge might be present is required. The effect of different sample rates is presented in chapter five through laboratory measurements in terms of phenomena detection.

For remote monitoring purposes, NETA-21 can create reports from the monitored data automatically. There are three different reporting methods available (ABB, 2014):

- Email reporting - reports are sent via email
- SD card reporting – reports are saved to an SD card
- FTP reporting – reports are transferred to FTP server

Reports are sent based on triggers. These triggers can be time intervals, parameter values or drive events. The best possible trigger for reporting depends on the fan or pump operation in place. For long-term monitoring, time interval -based report triggers might be the most applicable as they reduce the total number of reports. Also contamination buildup on the impeller is typically a slow process so we do not have to get report every time fan

has started to rotate; weekly or monthly reporting of the parameters might be sufficient. For the sake of testing the detection methods, reports are needed more frequently. This can be done by selecting short time interval for reporting. The shortest possible intervals are once every minute, every 5 minutes or every hour. If the fan or pump system is used seldom, then the reporting should be done every time there is new data available.

Format of the reports depends on what type of reporting method is used. Email reports can have an XML format (Figure 4.2) or a plain text format (Figure 4.3). User can also make a custom reporting format for email reports by using the web UI of NETA-21. JavaScript is used for formatting the reports. For reports stored to a SD card, the file format is either CSV or SQLite. SQLite report for parameter logging contains three different tables. Two of these are of interest in monitoring, *parameters*- and *value\_cache* -tables (Figure 4.4 & Figure 4.5). These tables provide information about logged parameters, their actual values and timestamps. The reports stored in FTP server are in CSV format.

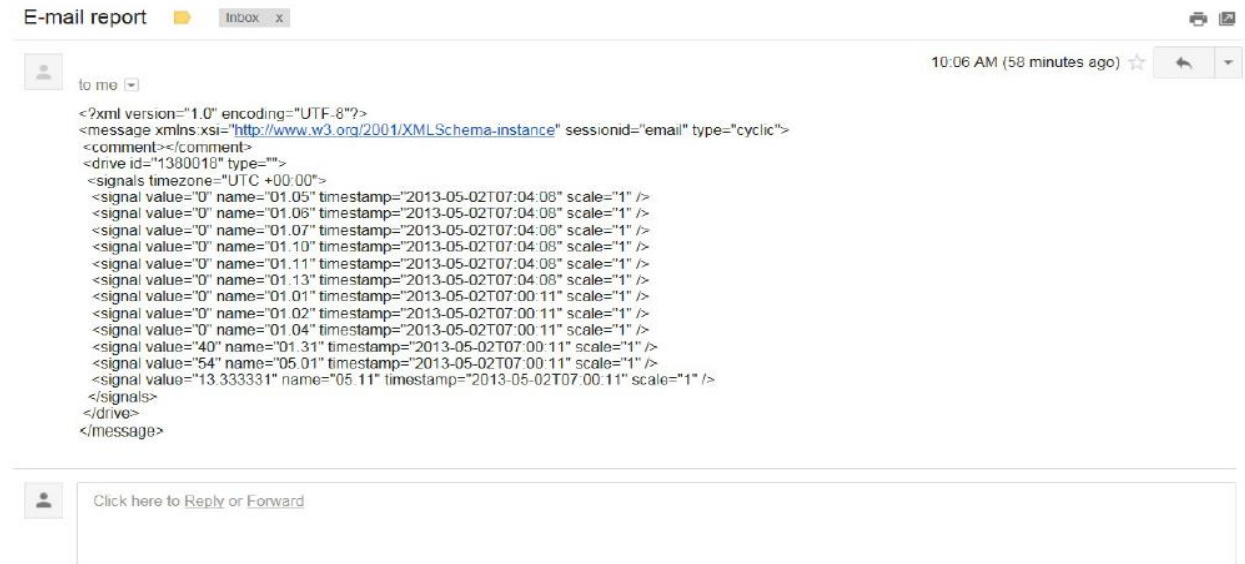


Figure 4.2 NETA-21 email report applying XML formatting (ABB, 2014).

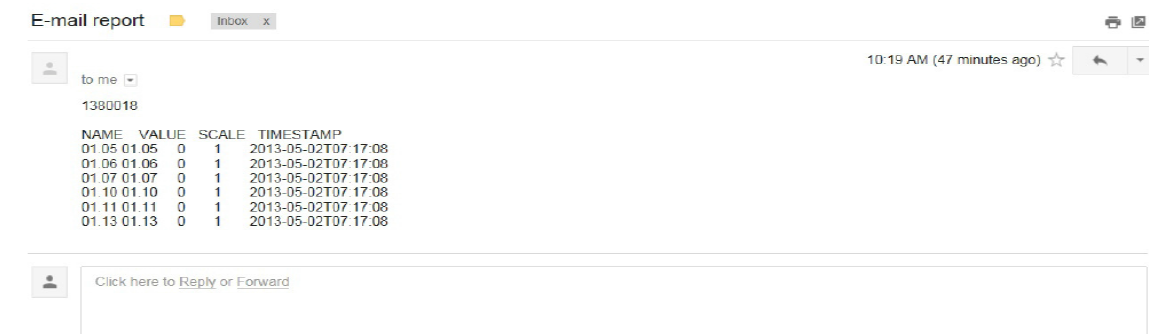


Figure 4.3 NETA-21 email report in plain text format (ABB, 2014).

id	node_id	signal_name
Filter	Filter	Filter
1	/eth/eth_192168000004_01/v/01.01	01_01_motor_speed_used
7	/eth/eth_192168000004_01/v/01.14	01_14_output_power
9	/eth/eth_192168000004_01/v/01.31	01_31_ambient_temperature
14	/eth/eth_192168000004_01/v/01.11	01_11_dc_voltage
57	/eth/eth_192168000004_01/v/01.02	01_02_motor_speed_estimated
60	/eth/eth_192168000004_01/v/01.07	01_07_motor_current
61	/eth/eth_192168000004_01/v/01.06	01_06_frequency
62	/eth/eth_192168000004_01/v/01.10	01_10_motor_torque

Figure 4.4 NETA-21 SD card report. Parameter table. This table shows which actual signal each id corresponds.

parameter_id	timestamp	value	type
Filter	Filter	Filter	Filter
1	1449125620020000	F1601.44543500000001.	2
57	1449125620040000	F1601.46142600000001.	3
60	1449125620413000	F7.705959.	3
61	1449125620544000	F53.3505210000000001.	3
7	1449125620670000	F1.834012.	3
62	1449125620789000	F56.6621090000000001.	3
14	1449125620910000	F562.004516999999996.	2
9	1449125621029000	F18.7795300000000001.	3
1	1449125621060000	F1599.73205600000001.	2

Figure 4.5 NETA-21 SD card report. Values table. This table shows parameter id and value of the parameter at given timestamp.

The default data monitoring allows continuous monitoring of the desired parameters with sampling time for a given parameter being between 1-30 seconds. For some systems this might be sufficient. However when there is a need for faster sampling rates, for example during a startup of a fan system, built-in device data loggers in a VSD can be utilized with NETA-21. Drives that are connected through DDCS protocol to the NETA-21 can have one or multiple device data loggers set up with up to 1000 Hz sampling frequency. The DDCS connection requires additional NEXA-21 module which can be easily installed to the NETA-21. The device data loggers are limited compared to the direct continuous monitoring as the device data loggers are filled quickly depending on the sampling rate and number of monitored parameters. After the logger has been filled, a report is created to the SD card of the NETA-21 and the data logging either stops or restarts depending on the used settings. However completely continuous uninterrupted monitoring is not possible.

While a frequency drive can be compatible with NETA-21, these device data loggers might not be accessible. Since it depends on the type of communication between the monitoring tool and drive, only the following drives can utilize faster trigger based logging: ABB ACS6000, ACS5000, ACS1000, ACS800, ACS600, ACX400, DCS800 and DCS600.

Start of the device data logging can set to be trigger based. With triggers we can monitor the drive parameters when there might be some phenomenon present to be detected in the system like cavitation or surge. This can be done by triggering the monitoring when a parameter reaches or falls below certain preset limit. For example, the data logging can be started just for startup of a fan system to monitor mass buildup over period of time. Manual triggering of the data logger through web UI (Figure 4.6) is also possible, but this requires personnel to start the logging and as such the automatic triggering conditions are more appealing when considering real applications outside of a testing environment. In the case of cavitation and surge detection, the reference values should be acquired first. This could be done with the manual triggering, but afterwards the data logging triggers can be set to be automatic. With the newest firmware version, data logging can also be triggered after certain time intervals for example every 5 minutes. This could also be used to detect the variation of the torque and rotational speed.

The screenshot shows a web interface for a device data logger. At the top, there are navigation tabs: 'Device front page', 'Parameter browser', 'Datalogger 1', 'Datalogger 2', and 'Events'. The 'Events' tab is active, displaying a table of events. The table has columns for Name, Local time, Relative time, Category, Source, and Severity. The events listed include status changes (running, stopped), datalogger uploads, and control actions (start, stop, triggered). Each event is timestamped and includes a relative time (e.g., '6 days 3 hours ago'). The severity of all events is 'notification'.

Name	Local time	Relative time	Category	Source	Severity
Status change: running	17.05.2016 11:47	6 days 3 hours ago	Device datalogger control	ib0ca9dca_02Datalogger1	notification
Status change: running	16.05.2016 11:12	7 days 4 hours ago	Device datalogger control	ib0ca9dca_02Datalogger1	notification
Status change: running	16.05.2016 08:36	7 days 6 hours ago	Device datalogger control	ib0ca9dca_02Datalogger1	notification
Status change: running	13.05.2016 11:32	10 days 3 hours ago	Device datalogger control	ib0ca9dca_02Datalogger1	notification
Status change: running	13.05.2016 09:56	10 days 5 hours ago	Device datalogger control	ib0ca9dca_02Datalogger1	notification
Status change: running	12.05.2016 14:35	11 days 49 minutes ago	Device datalogger control	ib0ca9dca_02Datalogger1	notification
Datalogger upload	12.05.2016 14:35	11 days 49 minutes ago	Device generated datalog	ib0ca9dca_02Datalogger1	notification
Status change: filed running	12.05.2016 14:35	11 days 49 minutes ago	Device datalogger control	ib0ca9dca_02Datalogger1	notification
Wrote control: start	12.05.2016 14:35	11 days 49 minutes ago	Device datalogger control	ib0ca9dca_02Datalogger1	notification
Status change: user_triggered filed	12.05.2016 14:35	11 days 49 minutes ago	Device datalogger control	ib0ca9dca_02Datalogger1	notification
Wrote control: trigger	12.05.2016 14:34	11 days 49 minutes ago	Device datalogger control	ib0ca9dca_02Datalogger1	notification
Status change: running	12.05.2016 14:34	11 days 50 minutes ago	Device datalogger control	ib0ca9dca_02Datalogger1	notification
Datalogger upload	12.05.2016 14:34	11 days 50 minutes ago	Device generated datalog	ib0ca9dca_02Datalogger1	notification
Status change: filed running	12.05.2016 14:34	11 days 50 minutes ago	Device datalogger control	ib0ca9dca_02Datalogger1	notification
Wrote control: start	12.05.2016 14:34	11 days 50 minutes ago	Device datalogger control	ib0ca9dca_02Datalogger1	notification
Status change: user_triggered filed	12.05.2016 14:34	11 days 50 minutes ago	Device datalogger control	ib0ca9dca_02Datalogger1	notification
Status change: user_triggered triggered running	12.05.2016 14:34	11 days 50 minutes ago	Device datalogger control	ib0ca9dca_02Datalogger1	notification
Wrote control: trigger	12.05.2016 14:33	11 days 50 minutes ago	Device datalogger control	ib0ca9dca_02Datalogger1	notification
Status change: running	12.05.2016 14:32	11 days 52 minutes ago	Device datalogger control	ib0ca9dca_02Datalogger1	notification
Datalogger upload	12.05.2016 14:32	11 days 52 minutes ago	Device generated datalog	ib0ca9dca_02Datalogger1	notification
Status change: filed running	12.05.2016 14:32	11 days 52 minutes ago	Device datalogger control	ib0ca9dca_02Datalogger1	notification
Wrote control: start	12.05.2016 14:32	11 days 52 minutes ago	Device datalogger control	ib0ca9dca_02Datalogger1	notification
Status change: user_triggered filed	12.05.2016 14:32	11 days 52 minutes ago	Device datalogger control	ib0ca9dca_02Datalogger1	notification
Status change: user_triggered triggered running	12.05.2016 14:32	11 days 52 minutes ago	Device datalogger control	ib0ca9dca_02Datalogger1	notification
Wrote control: trigger	12.05.2016 14:32	11 days 52 minutes ago	Device datalogger control	ib0ca9dca_02Datalogger1	notification
Datalogger upload	12.05.2016 14:31	11 days 53 minutes ago	Device generated datalog	ib0ca9dca_02Datalogger1	notification
Status change: filed running	12.05.2016 14:31	11 days 53 minutes ago	Device datalogger control	ib0ca9dca_02Datalogger1	notification
Wrote control: start	12.05.2016 14:31	11 days 53 minutes ago	Device datalogger control	ib0ca9dca_02Datalogger1	notification
Status change: user_triggered filed	12.05.2016 14:31	11 days 53 minutes ago	Device datalogger control	ib0ca9dca_02Datalogger1	notification
Wrote control: trigger	12.05.2016 14:30	11 days 53 minutes ago	Device datalogger control	ib0ca9dca_02Datalogger1	notification
Status change: running	12.05.2016 14:30	11 days 54 minutes ago	Device datalogger control	ib0ca9dca_02Datalogger1	notification
Datalogger upload	12.05.2016 14:29	11 days 54 minutes ago	Device generated datalog	ib0ca9dca_02Datalogger1	notification

Figure 4.6 The web UI for device data logger. Logging can be manually triggered or set to be automatic based on triggering conditions. These conditions include falling under or reaching over parameter threshold defined by the user or the logging can be triggered after certain time periods.

NETA-21 provides the necessary functionality for implementing a basic sensorless monitoring. As the data in the memory card can be accessed remotely, the phenomena detection can be done off-site with tools better suited for handling large quantities of measurement data.

## 4.2 Drive composer pro

As a DDCS connection between NETA-21 and a VSD is not always possible, another way to access the in-built data loggers and faster sampling rate is necessary. With ABB Drive composer pro software (DCP) the device data loggers can be accessed by establishing USB connection between PC and the VSD's panel bus.

DCP is a software tool designed by ABB. It allows a remote access to their VSDs. With

DCP the VSD can be controlled, adjusted and the required parameter estimates can be monitored and logged.

Data logging with DCP is simple to setup. Figure 4.7 shows the data logger view of the DCP. Sampling time can be controlled with a multiplier and a scalar value. Multiple signals can be chosen to be monitored from the drive's parameters and the program gives an estimate of the maximum sampling time with the current settings. Logged data can be stored as a CSV-formatted file.

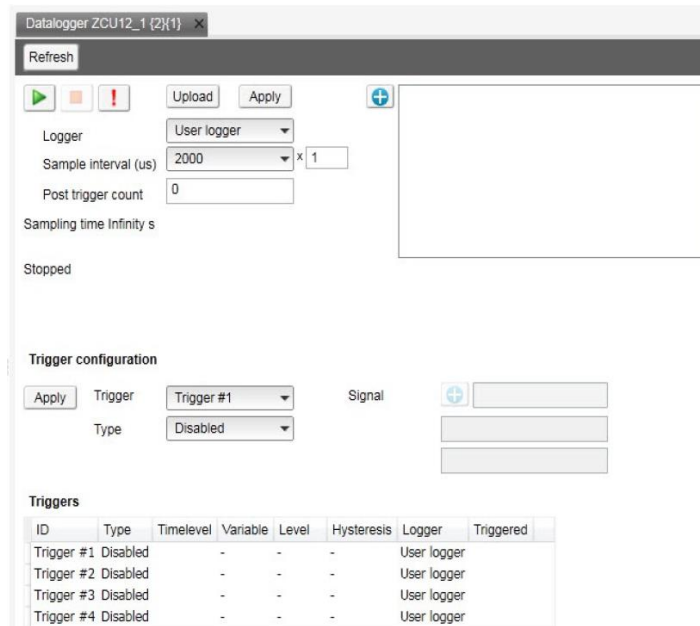


Figure 4.7 Data logger view of the DCP software. Setting up the data logger requires sampling interval and selecting the monitored signals.

Compared to NETA-21, DCP requires more user interactions, it has to be run on PC and it requires a physical connection with the VSD. Automatic data logging capabilities are also limited. This limits its usage purely as a monitoring tool. In this thesis it is still sufficient way to sensorlessly collect data with the VSD's data loggers and remotely detect harmful phenomena in a pump or a fan system.

### 4.3 Matlab

Analysis of the data gathered by NETA-21 and DCP was done with Matlab -software. Depending on the format of data files, Matlab can be directly used to open files, read the measurement data, plot it to figures and calculate necessary variables. These actions can be combined into single Matlab program files called scripts or m-files. Drawback of Matlab is that there is no possibility for real time remote monitoring software which could automatically fetch and analyze the report files. However in the scope of this thesis it is practical to use already available software rather than programming a completely new analysis tool from ground-up. Detection of deleterious phenomena can be done during a long time interval like in the case of impeller contamination so there is no need for real time monitoring in such cases and the detection methods can be applied to the collected data later on. General data analysis with Matlab for each of the phenomena will consists of following steps:

- NETA-21 is monitoring and storing the desired drive parameters, providing a report in a desired format. Various sampling times are tested to find suitable rates.
- Alternatively DCP is used for the same purpose if faster sampling rate is needed than what NETA-21 can provide.
- Matlab scripts are created to handle the report data. Afterwards, the script can be run with just new report files with no other changes necessary.
- Theory in chapter three is implemented through Matlab functions, which will provide the key variables for phenomena detection.
- The data is analyzed through these key variables and with figures plotted from the measurement data.

Objective is to make the data analysis universal so that the phenomena detection can be easily done in the future with just new report files. These steps combined with the theory in chapter three cover the basic functionality of the implemented sensorless, remote fluid system monitoring. Chapter five describes additional implemented functionality wherever it is required.

## 5 SENSORLESS PUMP SYSTEM MONITORING

Detection of cavitation and NRV condition were done in a pump laboratory at Lappeenranta University of Technology. The pumping system consisted of 11 kW induction motor (Figure 5.1), ABB ACS800 VSD (Figure 5.2), NETA-21 remote monitoring tool (Figure 5.3) and Sulzer AHLSTAR<sup>UP</sup> A22-80 centrifugal pump (Figure 5.4).

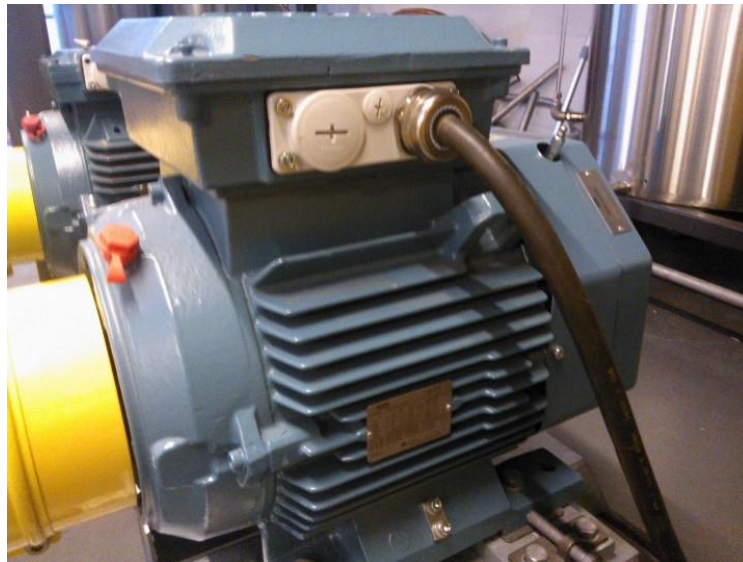


Figure 5.1 11kW ABB induction motor.



Figure 5.2 ABB ACS800 VSD.



Figure 5.3 ABB NETA-21 remote monitoring tool with additional NEXA-21 module. To access device data loggers, DDCS communication with the frequency drive was implemented by connecting NEXA-21 to the VSD with fiber optic cables. NETA-21 is connected to the laboratory network with Ethernet cable to gain access to the web UI and data logger settings.



Figure 5.4 Sulzer AHLSTAR<sup>UP</sup> A22-80 centrifugal pump.

Characteristic curves for the used centrifugal pump were provided by Sulzer Oy. From the flow-head curve (Q-H curve) in Figure 5.5 it can be seen how the impeller size affects the produced head and flow rate. The pump used in testing was equipped with a 265 mm diameter impeller. According to the Figure 5.5 the best operation point for this impeller size in this pump with a nominal rotational speed of 1440 rpm is between 35-40 l/s flow and 20-22 m of head. The current operation point can be estimated from the motor power measurement provided by the VSD. In the lower section of Figure 5.5 power, flow rate and impeller diameter are linked together in a flow-power curve (Q-P curve). At the best operation point, with the 265 mm impeller in use, approximate power would be around 9.5-10 kW. The operation point was also verified by measuring the flow rate with ABB

ProcessMaster 300 flowmeter and deriving the amount of produced head from the Q-H curve in Figure 5.5.

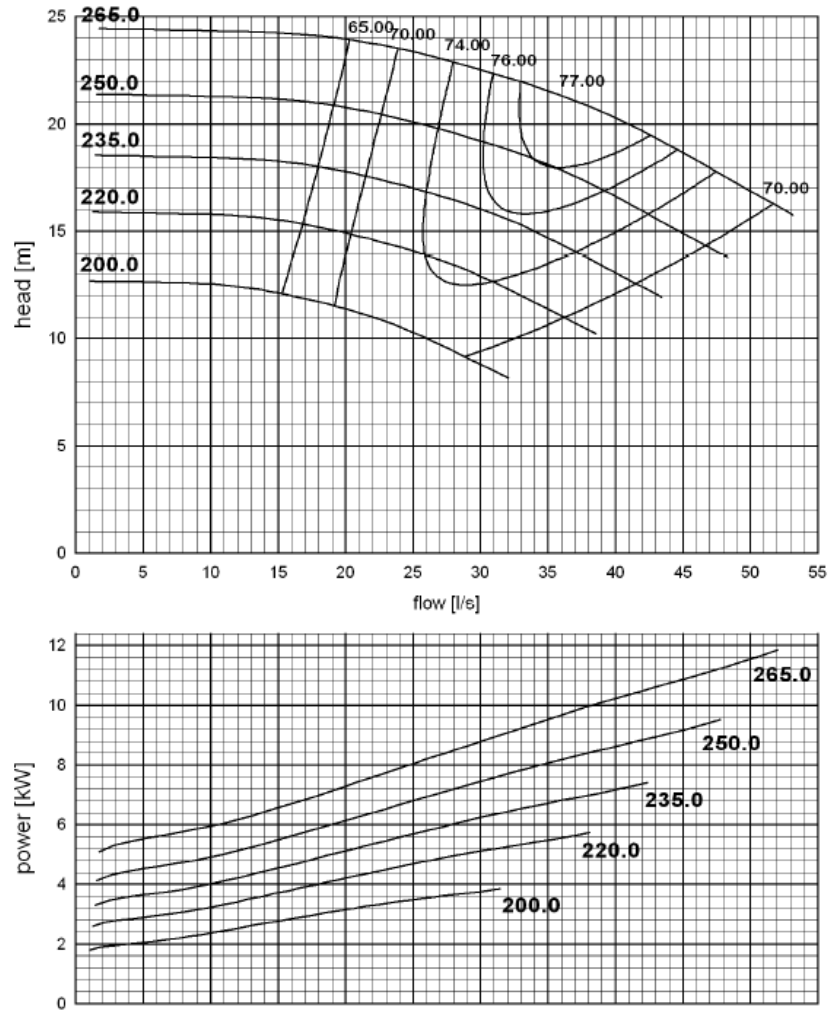


Figure 5.5 Q-H and Q-P curves for Sulzer AHLSTAR<sup>UP</sup> A22-80 centrifugal pump. Also shown are different impeller diameters and the pump efficiencies at different operating regions. The current operation point can be determined from power estimate or flow rate measurement.

### 5.1 Detecting cavitation

The entire pumping system is presented in Figure 5.6. The system made it possible to produce cavitation conditions by either lowering the available suction head  $NPSH_a$  or alternatively increasing the overall system friction and steepening the system curve by throttling a control valve at the pump discharge side. Both of these operations can lead to cavitation conditions in the system as stated in the chapter two. Aside from manually throttling a valve to control the  $NPSH_a$ , control of the pumping systems was done by using LabVIEW program. The program made it possible to control a valve position and to do automatic test runs by setting the valve position to a predefined value at a fixed time.

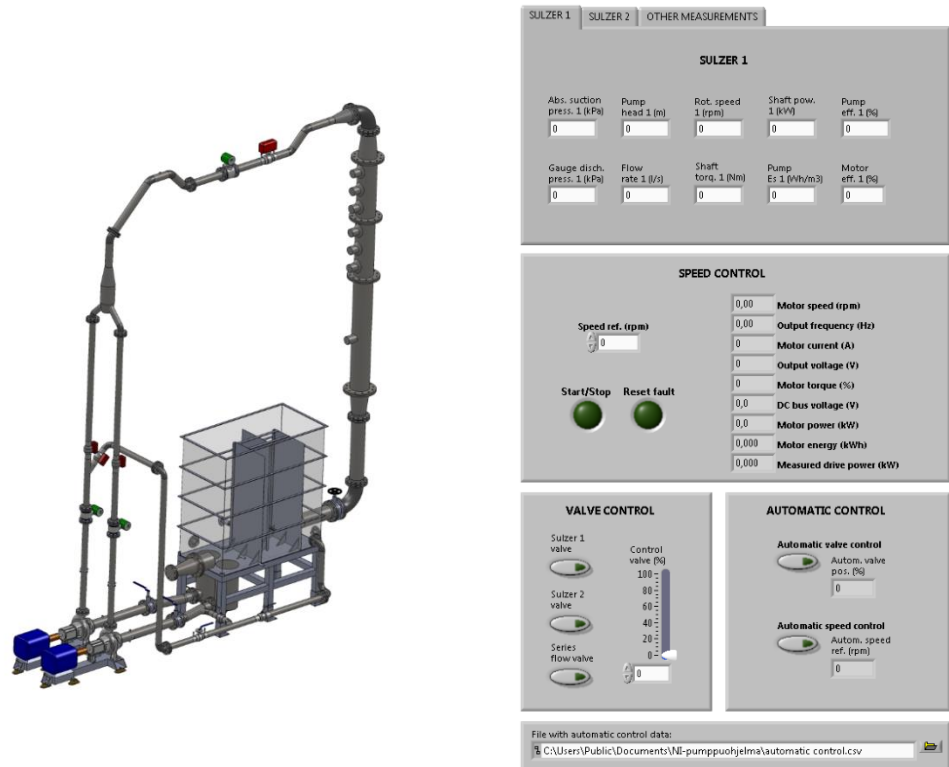


Figure 5.6 Pumping system used in the testing environment. While the figure shows two pumps and motors, only one pump-motor combination was in use during the testing. Current operation point can be controlled with either a manual throttling valve which is located between the water reservoir and the pump or by throttling a valve in the piping above the water tank by using a LabVIEW program.

The first objective in the cavitation detection testing was to see how the cavitation conditions could be initiated. As stated earlier, two possibilities existed in the testing system; either reducing the available suction head or increasing the amount of dynamic head. The reduction of suction head  $NPSH_a$  was tested first as it was also the method used in (Ahonen, 2011a) to induce cavitation conditions. For this, the required suction head  $NPSH_r$  at the current operation point has to be known. Pump manufacturers typically provide a characteristic  $NPSH_r$  curve. Figure 5.7 shows the  $NPSH_r$  curve for the pump used in testing.

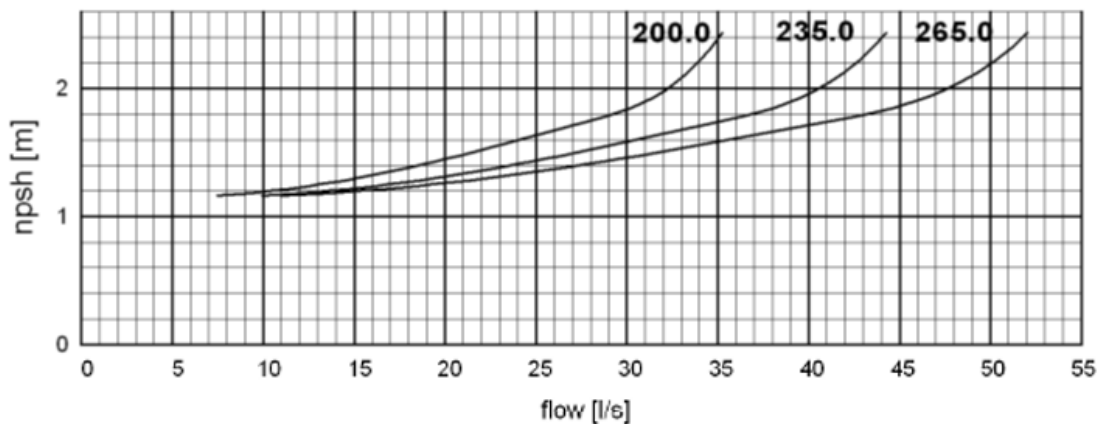


Figure 5.7  $NPSH_r$  of the Sulzer AHLSTAR<sup>UP</sup> A22-80 pump.

As the pump had an impeller with 265 mm diameter, the  $NPSH_r$  at the best efficiency point (35-40 l/s) when utilizing nominal speed is approximately 1.6 meters. The  $NPSH_a$  could be controlled with a throttling valve between the water reservoir and the suction side of the pump. Current  $NPSH_a$  was measured from the suction side pressure which was converted to meters of head with equation

$$NPSH_a = \frac{p}{\rho g}, \quad (15)$$

where  $p$  is the pressure at the suction side (Pa),  $\rho$  is the density of the fluid (ca. 1000 kg/m<sup>3</sup> for water) and  $g$  is acceleration due to the gravity (9,81 m/s<sup>2</sup>). With fully open suction side valve, the calculated  $NPSH_a$  was 11.0 meters. This is more than enough for any operation point defined by the characteristic curves as the maximum  $NPSH_r$  in Figure 5.7 is 2.4 meters. The suction valve had 10 possible positions from fully open to completely closed (Figure 5.8). With rough control like this, precise adjustment of the  $NPSH_a$  was not possible. Because of this, the ratio between  $NPSH_a$  and  $NPSH_r$  was either well over 1.35 (Karassik, 1998 & Ahonen, 2011a) or severely under it. As such only two very clear cases of operation were available and there would be no uncertainty of cavitation.



Figure 5.8 Manual throttling valve at the suction side of the pumping system. The valve had 10 possible positions ranging from fully open to completely closed valve. The amount of  $NPSH_a$  can be reduced by closing the valve.

If the ratio between available and required suction head could be controlled more precisely then this method could be used for testing cavitation detection. As it was not the case the reduction of suction side pressure was dismissed. Cavitation conditions were ultimately caused by throttling a control valve thus increasing the system friction and moving the current operation point away from the BEP.

(Ahonen, 2011a) shows that the cavitation increases the amplitude of low frequency components of the measured rotational speed and torque signals. This low frequency region is stated to be between 0-10 Hz. Thus at least 20 Hz sampling frequency is required to cover the entire bandwidth. NETA-21 has an option for continuous monitoring which

has the fastest sampling rate setting at one sample per second (1 Hz). On the other hand ACS800 has two build-in data loggers which the NETA-21 can access. These data loggers can have sampling frequency up to 1000 Hz. However they are limited by the length of the data logger. To find a fitting sampling rate, the device data loggers were tested with different frequencies while monitoring torque and rotational speed at two different operation points, which are a point in best efficiency region referred to as 'BEP' and a point outside of best efficiency region referred to as 'Not BEP'. From rotational speed, filtered and unfiltered estimates were monitored (parameters 1.02 MOTOR SPEED FILT and 02.17 SPEED ESTIMATED in the VSD). In actual cavitation detection testing only one of these is required. Results with different sampling frequencies are seen in the following figures.

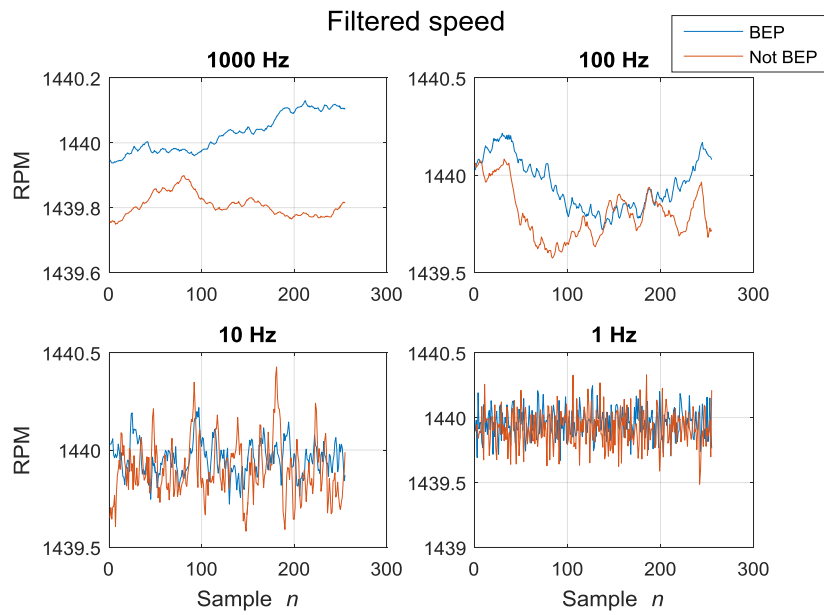


Figure 5.9 Measured filtered rotational speed values during a single logging interval.

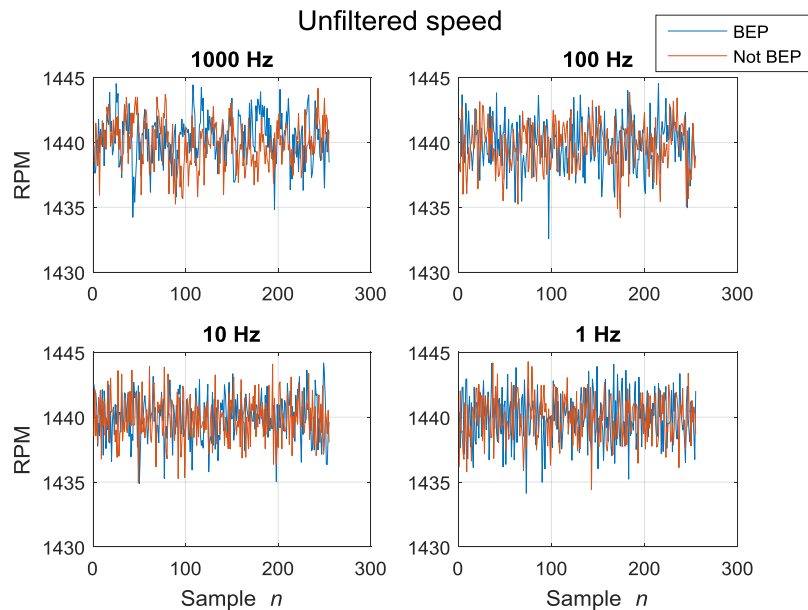


Figure 5.10 Measured unfiltered rotational speed values during a single logging interval.

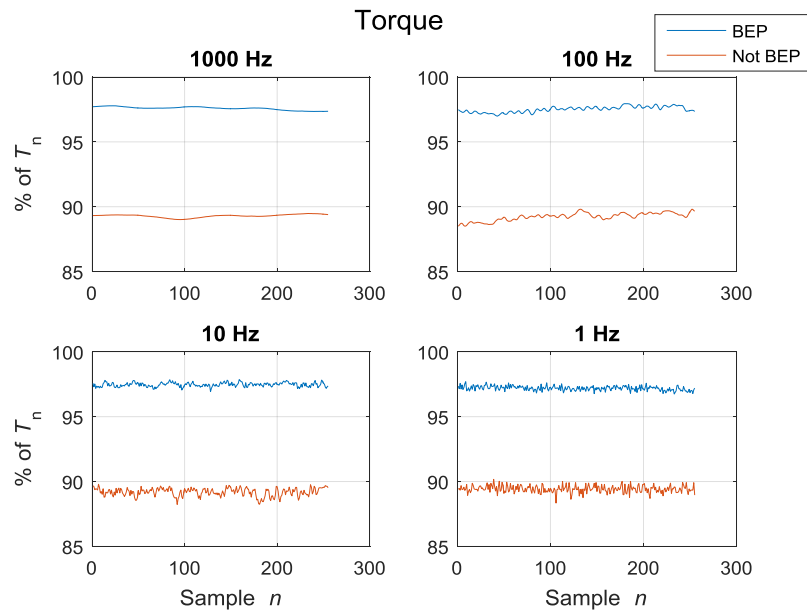


Figure 5.11 Measured torque values during single logging interval. Torque is presented as percent of the nominal torque  $T_n$ .

From these figures it can be seen that the number of samples stored during a single logging interval with three parameters is approximately 250. The used sampling rate does not affect this value at all. Thus with a 1000 Hz sampling frequency we get measurements during a quarter of a second. As the fluctuations in measured signal happen in a low frequency region this duration is not enough as the measurement should last several seconds for there to be noticeable fluctuations. In Figure 5.9 and Figure 5.11 it can be seen that there are hardly any variation differences between the two operation points with 1000 Hz sampling frequency. With 100 Hz sampling frequency the overall sampling time is tenfold compared to the 1000 Hz, netting a total sampling time of 2.5 seconds. With this frequency, the measured signals start to include visible vibration in them, especially the unfiltered speed estimate in Figure 5.10. However the difference between the two operation points is not clearly visible. Also in Figure 5.9 and Figure 5.11 the sampling frequency seems still too high with no clear sign of increase vibration amplitude when moving away from the BEP. With 10 Hz and 1 Hz the effect of moving the operation point away from the best efficiency region starts to look clearer. There is a noticeable variation in the measured estimates and the amplitude of the variation increases when the pump is operating away from the BEP. This suggests that the continuous monitoring could be used for cavitation detection with NETA-21 as it's capable of 1 Hz sampling frequency. If the device data loggers are used then the sampling frequency can be somewhere between 10-100 Hz at maximum. Cavitation causes low frequency vibrations in region of 0-10 Hz so sampling frequency of 20 Hz could be used as a starting point if one wants to use maximum frequency with the device data loggers to detect cavitation. This would allow sampling time to be 12.5 seconds with three monitored parameters which should be sufficient for cavitation detection.

With an idea of the maximum sampling frequency, cavitation detection was tested with VSD's build-in data logger by increasing the system friction and thus moving the operation point further away from the BEP. All of the operation points used in the testing are

presented in Figure 5.12 as intersections between each system curve and Q-H curve of the pump. The Q-H curve is based on the manufacturer provided curve for 265 mm impeller seen in Figure 5.5. The system curves were calculated with equation

$$H = H_{st} + kQ^2, \quad (16)$$

where  $H_{st}$  is static head,  $k$  is system friction and  $Q$  is flow rate. Static head was set to 10 meters and  $k$  was solved from (16) by having measured flow rate and assigning correct amount of total head  $H$  from Figure 5.5 depending on the flow rate.

The control valve was closed from 100 % to 35 % open with 5 % point intervals (Figure 5.12). As seen in Figure 5.12, at the first three operation points (valve position from 100 % to 90 % open) there is practically no effect on the system curve. Further closing the control valve moves the operation point away from the best efficiency region towards the cavitation conditions. In the chapter two it was stated that the low flow cavitation begins to occur when the pump efficiency has been reduced by 10 % points. Deriving from the efficiencies shown in Figure 5.5, this would happen when the flow rate is nearing 20 l/s. This happens approximately when the valve is 70 % open. From this information it can be concluded that the reference values for torque and rotational speed variations should be obtained when the valve is nearly completely open, the threshold ratio for cavitation detection should be noticeable when the valve is 70 % open and the cavitation should be clearly detectable from the measurements when the valve is 35 % open.

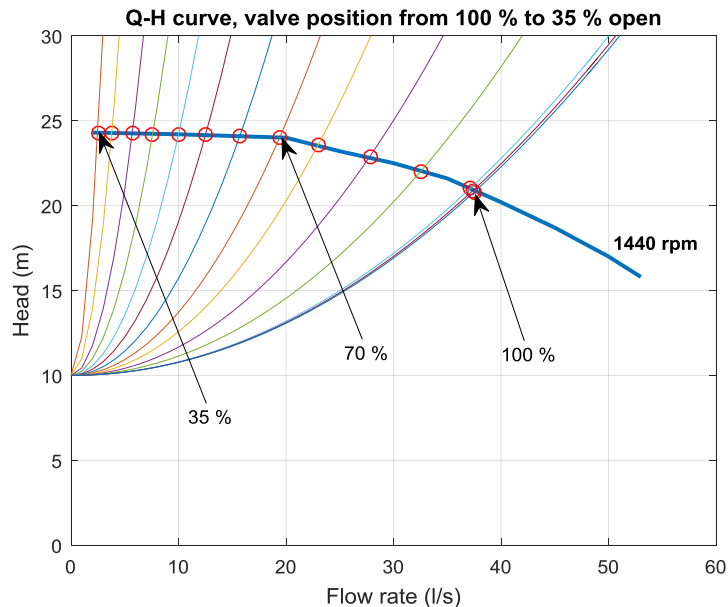


Figure 5.12 System curves and Q-H curve of the pump. By closing a control valve, the current operation point can be changed. Cavitation begins to occur when the valve is 70 % open.

Testing of cavitation detection was done by manually triggering the VSD's data loggers through NETA-21 web UI and logging torque and rotational speed estimates at each valve position. RMS values were calculated with equations (1), (2) and (3). Rotational speed remained the same during the testing at 1440 rpm. As the amount of required torque changed depending on the operation point, the RMS values for torque were scaled according to their DC levels to make the results comparable. The figures below present the results such that there is the RMS ratio for each parameter at each valve position. The

reference value was set to be the lowest amount of variation and the rest of measured RMS values were compared with it.

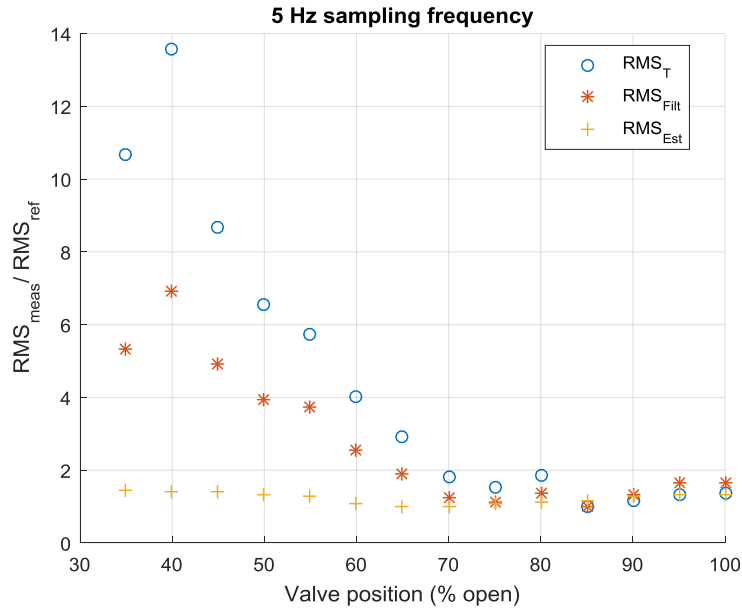


Figure 5.13 Cavitation detection test done with 5 Hz sampling frequency. Three parameters are monitored: torque, filtered rotational speed and unfiltered rotational speed. The lowest RMS values are used as references for the rest of the measurements.

In Figure 5.13 results from the cavitation detection test are shown. Monitoring was done with a 5 Hz sampling frequency while measuring three parameters. It can be seen that at the predicted valve position of 70 % open, there is almost twice as much variation in torque. On the other hand the rotational speed estimates don't show that much increase at this operation point. When further closing the valve the RMS ratios for torque and filtered speed estimate start to rapidly increase. Amount of variation in the unfiltered speed estimate seems to be unaffected throughout the entire test.

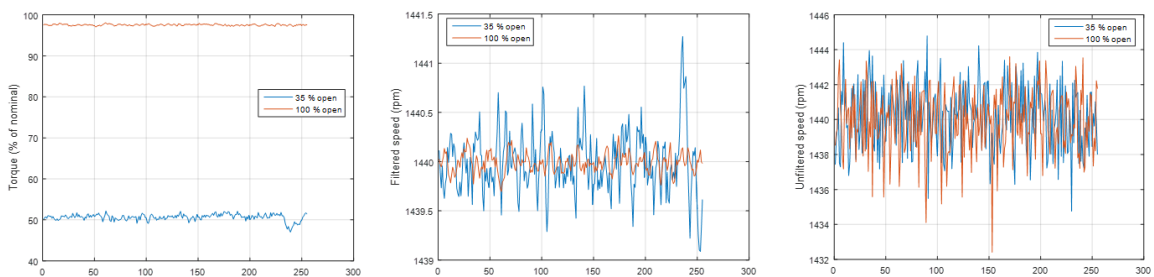


Figure 5.14 Measurement data with 100 % and 35 % open control valve. The difference in variation in these two cases is clear with torque and filtered rotational speed. There is hardly any difference in unfiltered rotational speed values.

Figure 5.14 shows the measured data when the pumping system is operating within its best efficiency region (100 % open valve) and when cavitation is clearly present (35 % open valve). For torque and filtered rotational speed there is a clearly visible difference between these two operation points in terms of vibration amplitudes. With unfiltered speed the difference is unnoticeable. This suggests that the monitored parameters for cavitation detection should be filtered rotational speed and torque.

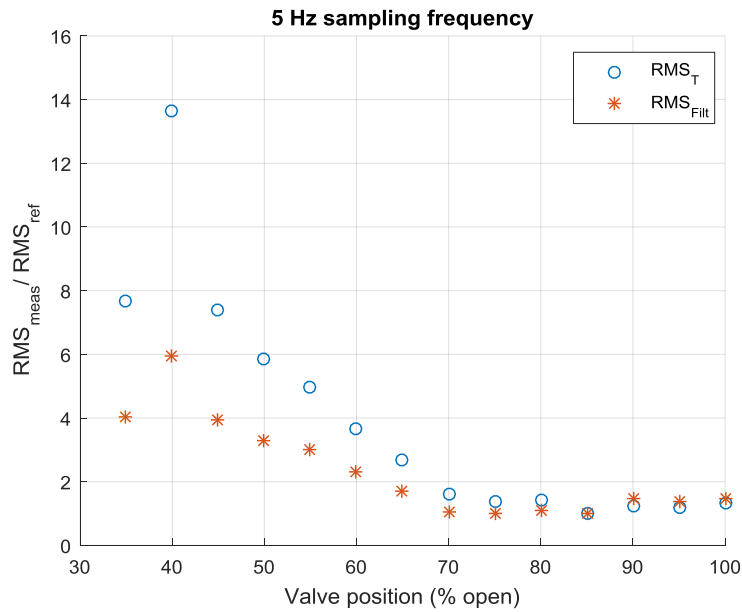


Figure 5.15 Cavitation detection test with 5 Hz sampling frequency. Two parameters are monitored: torque and filtered rotational speed. The lowest RMS values are used as reference point for the rest of the measurements.

Same test was repeated while monitoring only two parameters: filtered rotational speed and torque (results in Figure 5.15), as these two were the only parameters affected by cavitation. Now the amount of samples for each measured parameter doubled from the previous 250 samples which were gained when measuring three parameters. This time the RMS ratios were lower but cavitation could still be detected from the same operation points as before.

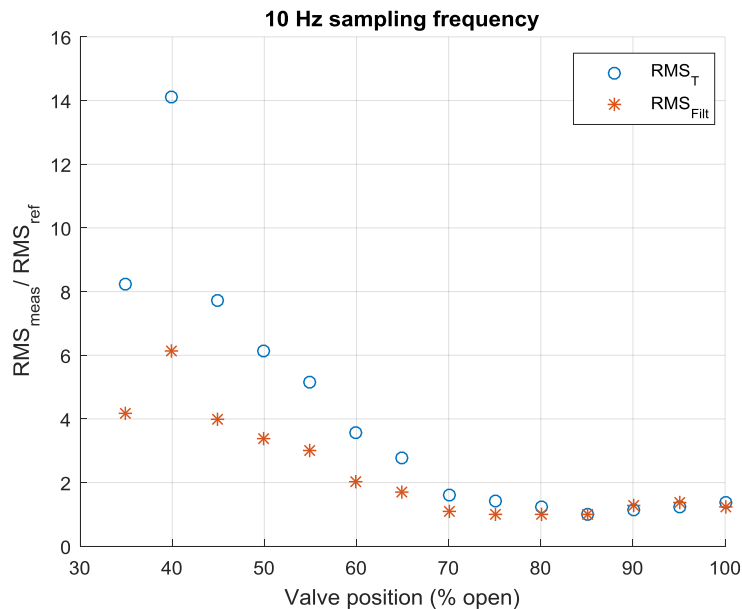


Figure 5.16 Cavitation detection test with 10 Hz sampling frequency. Two parameters are monitored: torque and filtered rotational speed. The lowest RMS values are used as reference point for the rest of the measurements.

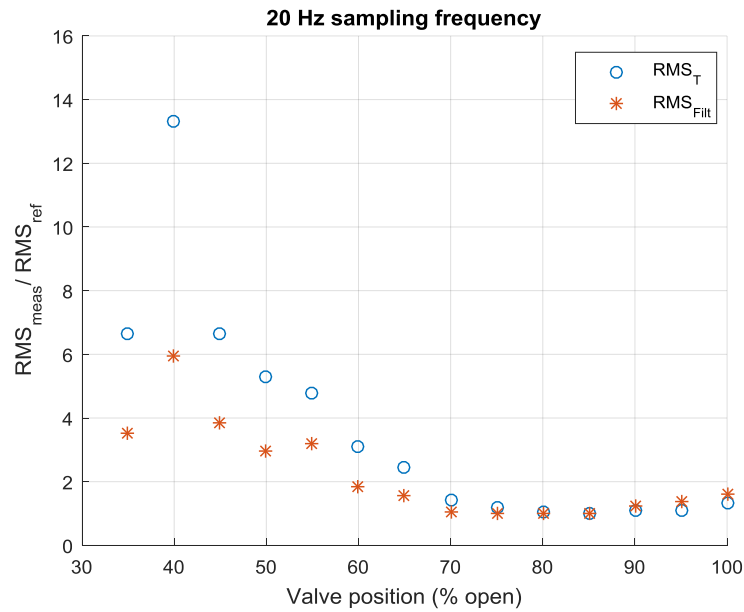


Figure 5.17 Cavitation test with 10 Hz sampling frequency. Two parameters are monitored: torque and filtered rotational speed. The lowest RMS values were used as reference point for the rest of the measurements.

Figure 5.16 and Figure 5.17 show the results from cavitation detection test with two parameters while using higher sampling frequencies. The results are similar to the ones presented in Figure 5.15 with minor differences in the measured RMS ratios. VSD’s own data loggers seem to be applicable for cavitation detection when monitoring filtered speed and torque. The sampling frequency should not be too high as the length of the data logger limits the amount of gathered samples and sampling time too much with high frequencies.

Next the possibility of continuous monitoring with NETA-21 was tested. Potential drawbacks of this type of monitoring are the low sampling frequencies and the gathered data has to be handled differently because the cavitation detection is done when the pump is operating in a steady state so the possible transient operation states have to be excluded from the measured data. The continuous monitoring was tested by automatically running an hour-long pumping process where the control valve closes step-by-step to the 35 % open state and afterwards opens back to starting position, again in a step-by-step fashion. Valve positions during the process can be seen in Figure 5.18.

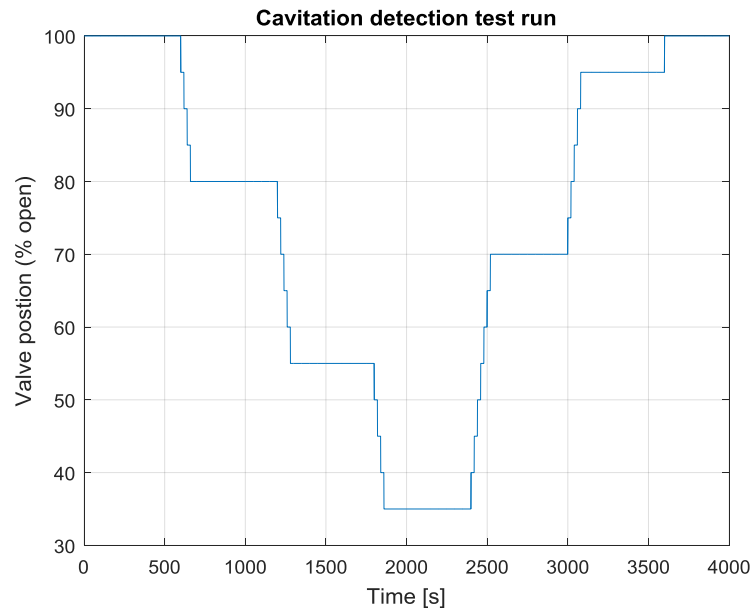


Figure 5.18 Valve position during the cavitation detection test run. The process begins with the control valve 100 % open. In the middle of the process the valve has closed down to 35 % open. In the end the valve has been opened back up to 100 % open position.

In this chapter it has been stated that the 70 % open valve position marks the beginning of the cavitation in the testing environment. From the seven steady states seen in Figure 5.18, two fall under this limit (55 % and 35 %) and cavitation should be detected clearly from those states. One state is exactly at the 70 % mark and the cavitation may be detectable depending on what ratio is chosen between the measured and reference RMS values. Figure 5.19 shows the measured torque during the test run. Steady state operations are marked as red and the RMS values are calculated from these areas.

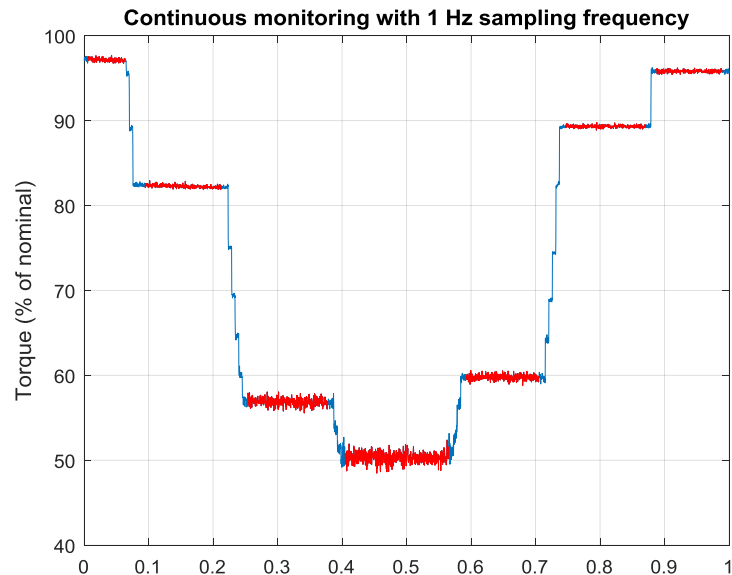


Figure 5.19 Torque estimates from continuous monitoring with 1 Hz sampling frequency. An increase in the variation amplitude of the measured signal is clearly seen at the red-marked steady state areas as the operation point moves away from BEP. All transient states are excluded when calculating the RMS values and as such there will be seven separate entities for which the cavitation detection algorithm is applied.

The detection of steady state from the measurement data is based on moving average filtering. This allows detection of the steady states even when there exists high amount of variation during the steady operation. Other benefit of the steady state recognition is that we don't have to have any prior knowledge about the actual process being measured. Only torque and speed measurements are required for cavitation detection. Simplified algorithm for steady state recognition from continuous measurement data is described in Figure 5.20.

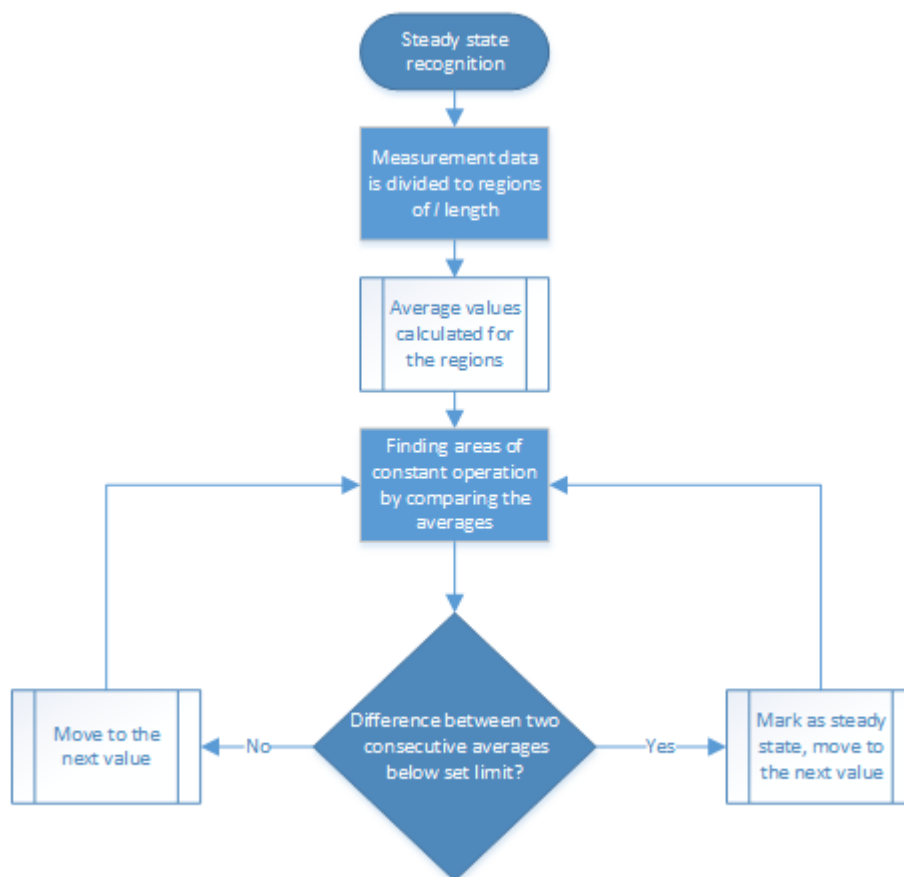


Figure 5.20 Simplified flow chart for steady state recognition from continuous measurement data. Recognition was implemented as Matlab function.

After the steady state areas have been recognized from torque measurements, these same areas can be marked from rotational speed data as seen in Figure 5.21. Even though the rotational speed remains constant during the entire test process, we can track down the areas from which the RMS values should be calculated.

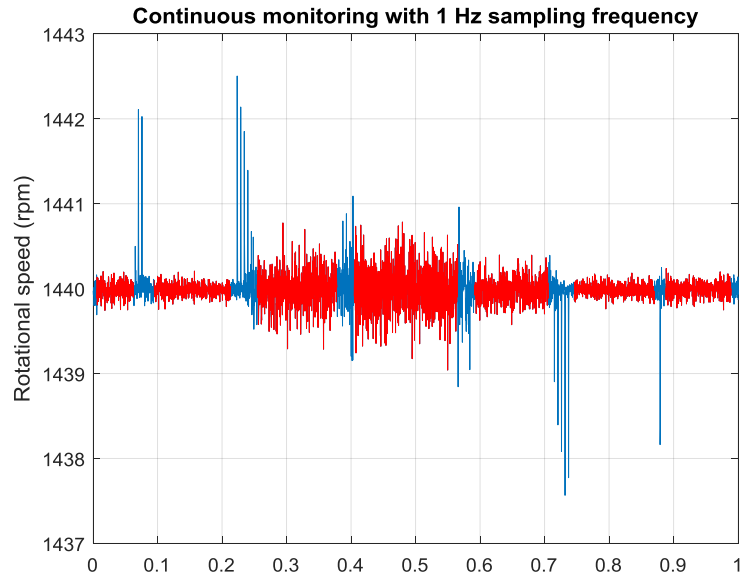


Figure 5.21 Rotational speed measurements from the continuous monitoring with 1 Hz sampling frequency. After the areas of steady operation has been recognized from the torque data, these same areas can be found and marked from the speed measurements.

Results from the continuous monitoring are presented in Table 1. The lowest RMS values are used as references,  $T_{rms,ref}$  and  $n_{rms,ref}$ , which are indicating the variation amplitude in normal operating conditions when cavitation is not present.

Table 1 Results from cavitation detection test while using continuous monitoring with 1 Hz sampling frequency.

Valve position	$T_{rms,meas}$	$T_{rms,meas}/T_{rms,ref}$	$n_{rms,meas}$	$n_{rms,meas}/n_{rms,ref}$
100	0.0019	1.27	0.0642e-3	1.35
80	0.0021	1.40	0.0491e-3	1.04
55	0.0074	4.93	0.1480e-3	3.12
35	0.0115	7.67	0.1913e-3	4.04
70	0.0049	3.27	0.0970e-3	2.05
95	0.0015	1.00	0.0474e-3	1.00
100	0.0016	1.07	0.0562e-3	1.19

Cavitation is clearly detected when valve position is at 55 % or 35 % open. If using a threshold ratio of 2.0 for both the torque and rotational speed, cavitation is also detected when the valve position is at 70 % open as the  $n_{rms,meas}/n_{rms,ref}$  barely crosses this limit. Continuous monitoring with 1 Hz sampling frequency seems like a viable option for cavitation detection based on these results. Compared to the trigger based data logging with short measurement intervals, more computations are needed with continuous monitoring as the areas of steady operation have to be found from the collected data. Continuous monitoring can also consume more memory space.

Cavitation detection was also tested with trigger-based device data loggers having 20 Hz sampling frequency. As the test run was a bit more than hour-long and the areas of constant operation were between 5-10 minutes in duration, the data logger was set to

trigger every 5 minutes. If the logging happened during a transient process state, the report file was ignored. Results from the test run are presented in Table 2.

Table 2 Results from cavitation detection test while using timed triggering of VSD's device data loggers utilizing 20 Hz sampling frequency.

Valve position	$T_{rms,meas}$	$T_{rms,meas}/T_{rms,ref}$	$n_{rms,meas}$	$n_{rms,meas}/n_{rms,ref}$
100	0.0019	1.06	0.0686e-3	1.18
100	0.0018	1.00	0.0636e-3	1.09
100	0.0022	1.22	0.0599e-3	1.03
80	0.0024	1.33	0.0637e-3	1.09
-	-	-	-	-
55	0.0074	4.11	0.1536e-3	2.64
55	0.0123	6.83	0.2124e-3	3.65
35	0.0118	6.56	0.2091e-3	3.59
-	-	-	-	-
70	0.0053	2.94	0.1072e-3	1.84
-	-	-	-	-
95	0.0018	1.00	0.0582e-3	1.00
95	0.0018	1.00	0.0790e-3	1.36

The blank rows are the ignored report files as the logging happened during a transient state. From the measurements occurring during steady pumping process it can be seen that the amounts of variation in torque and rotational speed are of the same magnitude as they were when the monitoring was done continuously with 1 Hz sampling frequency (Table 1). When looking for more exact information about when the cavitation has occurred, timestamps can be looked up from the measurement files which have been taken during cavitation. In this case, current valve position was determined from timestamps.

Comparing continuous monitoring and trigger based monitoring, both have their benefits. With trigger based monitoring, extra algorithms for finding the areas of steady operation are not needed because there are multiple measurement files. The sampling time is short and the measurement can set to happen for example every five minutes. Some form of check on the data is still necessary, so the data collected during transient operation can be dismissed. This may be simply just averaging the data and comparing the first and the last samples of the measured parameter with it. With continuous monitoring, the logged data can be used for other purposes as well instead of just cavitation detection, as there is knowledge on torque and rotational speed at all times instead for just a few seconds every couple of minutes.

## 5.2 Detecting NRV breakdown

NRV breakdown detection was based on measurements done in the same pumping laboratory using the same setup as with the cavitation detection. Data for the reference shutdown behaviour with a working NRV was available from a previous research done in

(Ahonen, 2015). NRV malfunction was simulated by monitoring the shutdown behaviour of the system when there was no NRV installed. This shutdown behaviour would then be compared with the existing data to detect a faulty NRV operation. Original, working shutdown behaviour can be seen in Figure 3.6. In the original research, the VSD in use was ACS880 as opposed to the current test setup with ACS800. This might affect the results, as the VSD's shutdown settings cannot be replicated entirely thus the shutdown procedure may not be completely identical.

The shutdown behaviour was monitored with NETA-21 by utilizing trigger based data loggers of the VSD with 8 ms sampling interval as the same interval was used in previous research in (Ahonen, 2015). The logging was set to start when rotational speed falls below 500 rpm threshold with 300 samples stored pre-triggering to capture the complete shutdown behaviour. The shutdown behaviour with working NRV and without NRV can be seen on Figure 5.22. There are two curves for pump shutdown without NRV and one with NRV installed. The two test runs without NRV provided similar results. There is a notable difference in the measured torque when comparing the reference behaviour with the test runs. While the curve shapes are similar, there is more torque provided when NRV is stuck open.

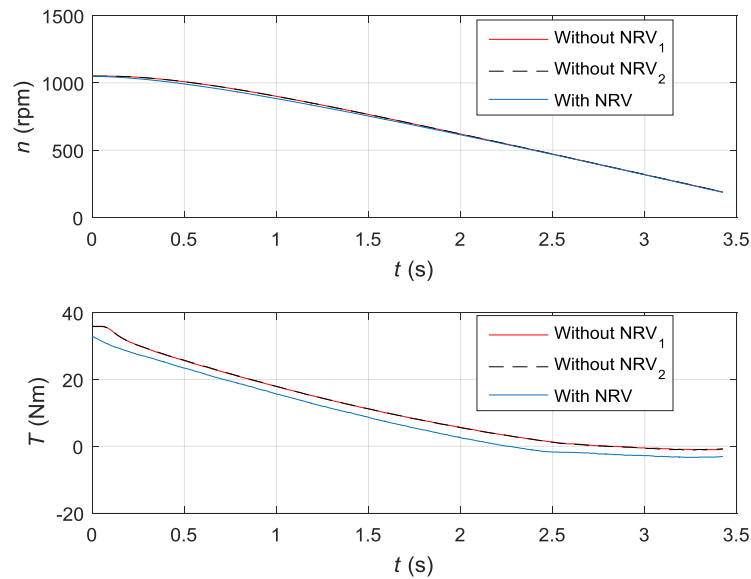


Figure 5.22 Shutdown behaviour of the monitored pumping system. Two curves are from measurements when NRV was not installed and one is from the data gathered in (Ahonen, 2015). The rotational speeds are practically identical when the system is shutdown with 3.5 second long deceleration ramp. When NRV is not installed (simulated fault in NRV), torque decelerates more slowly than it would with working NRV.

Figure 5.23 shows close-up of the area from which the produced torque sum is calculated. It starts from 500 rpm and continues until the VSD stops modulating and providing parameter estimates. Without NRV there is higher amount of produced torque which is needed to realize the desired shutdown behaviour.

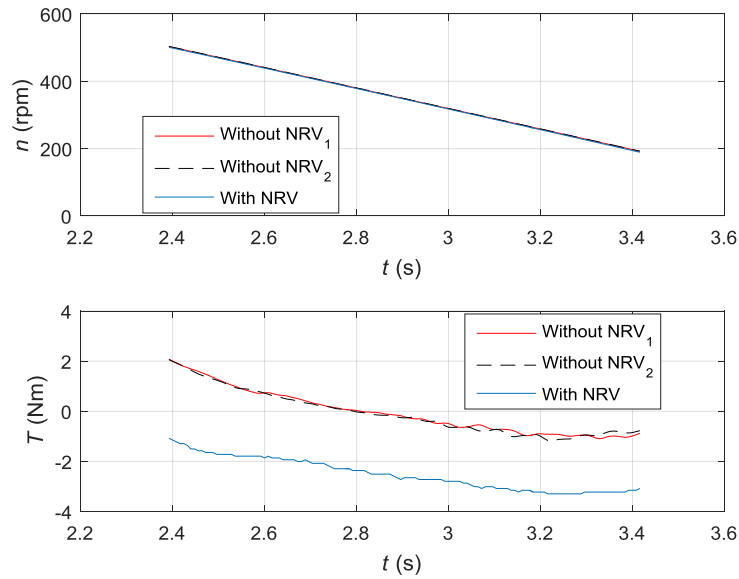


Figure 5.23 Closer view on the shutdown behaviour. Torque sum is calculated from this data set to see whether or not the shutdown behaviour has changed due to a NRV malfunction.

Behaviour of the torque estimate when NRV is not installed in Figure 5.23 does not appear to be the same as in Figure 3.7 where the amount of torque increased at the end of the measurements. This may be because a different VSD was used and therefore the shutdown was not completely identical due to different shutdown parameters. Resulting cumulative torque sum for the reference behaviour was  $\sum T_{est,ref} = -324.2$  and the sums when NRV was open were  $\sum T_{est,1} = -9.3$  and  $\sum T_{est,2} = -13.7$ . These results would suggest that the condition of a NRV could be monitored and possible breakdown can be sensorlessly detected when the correct behaviour is known.

## 6 SENSORLESS FAN SYSTEM MONITORING

Sensorless fan system monitoring was done at Lappeenranta University of Technology. The setup fan system consisted of FläktWoods Centripal EU 4 MD 630 radial blower (Figure 6.1), 7.5 kW induction motor, ACS800 VSD and NETA-21 remote monitoring tool. Nominal rotational speed was 1450 rpm.



Figure 6.1 FläktWoods Centripal EU 4 MD 630 radial blower in a test setup. Flow measurement is done from the suction side and the operation point is controlled with a damper at the discharge side of the system.

This setup was used for both detecting surge and noticing contamination buildup on the fan impeller. Current operation point was approximated by having a measured flow rate from suction side of the fan and comparing it to the characteristic curve (Figure 6.2) provided by the fan manufacturer (Fläkt Woods, 2016). The flow rate measurement was done with Eldridge 9800MPNH flow meter (Eldridge, 2016).

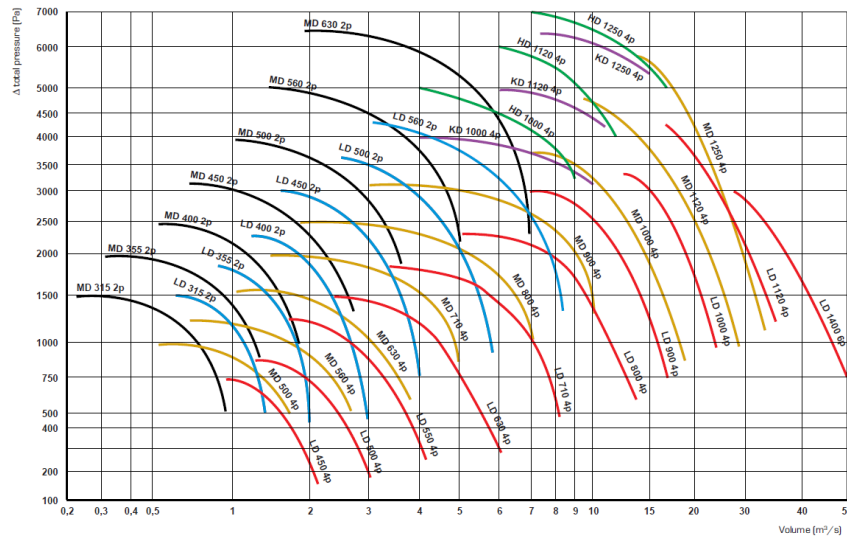


Figure 6.2 Q-P curves provided by manufacturer for Centripal EU 4 fans. Curve labeled as MD 630 4p represents the nominal curve for the fan used in testing.

## 6.1 Detecting surge

Surge detection was done according to the theory presented in chapter 3.2.2. The fan was run with a nominal rotational speed of 1450 rpm at different operation points. Location of the current operation point was controlled with a damper at the fan discharge side. Flow rate at each point was measured and the operation points were estimated accordingly and fitted to the fan's Q-H curve (Figure 6.3).

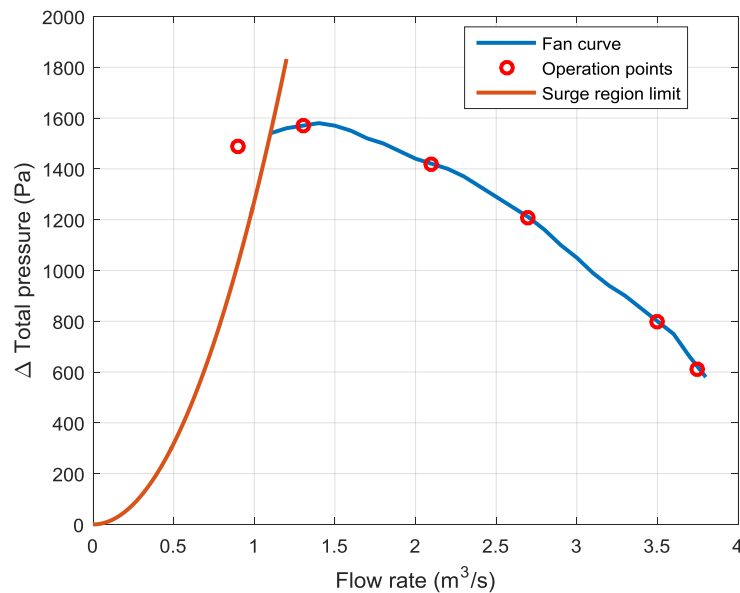


Figure 6.3 Estimated operation points on the Q-H curve. Operation points were estimated from measured flow rate. One operation point is on the left-side of the surge region limit indicating possibility of surge detection.

From these operation points, only the leftmost point ( $0.9 \text{ m}^3/\text{s}$  flow and 1490 Pa) is outside of the manufacturer's curve. This area is labeled as surge region as the pressure generated

by the fan starts to decrease with lower flow rates and possibility of surging increases.

Unfiltered torque and rotational speed estimates (parameters 1.10 MOTOR TORQUE and 01.2 MOTOR SPEED ESTIMATED in the VSD with the default filter time constant set to minimum) were monitored when the fan was operating steadily at each of the operation points. From the measured torque and speed estimates,  $T_{rms}$  and  $n_{rms}$  were calculated. The lowest calculated RMS values were used as references for how much there is variation in torque and speed when the fan is operating outside of surge region, possibly near the BEP. Surge detection variable  $S$  was calculated according to equation (6).

Since DDCS connection between NETA-21 and ACS880 was not possible, fast data logging (>1 Hz sampling frequency) was done with DCP. For slower data logging with sampling interval of 1 second or higher, NETA-21 was used.

Results with 50 Hz sampling frequency are presented in Table 3. Flow rate denotes the operation point in question. RMS values presented in the table were calculated by having five measurement sets at each of the operation points, calculating  $T_{rms}$  and  $n_{rms}$  from each set and taking a mean value from them.

Table 3 Results from surge detection method with 50 Hz sampling frequency. RMS values were calculated as mean values from five measurement sets at a single operation point. Threshold for surge detection can vary but in this case  $S > 2$  could be used to notice surging.

Flow rate $Q$ ( $m^3/s$ )	Torque variation $T_{rms}$	Standard deviation for torque variation	Rotational speed variation $n_{rms}$	Standard deviation for rotational speed variation	Surge detection variable $S$
0.9	0.0228	0.0014	0.0011	0.78e-4	2.25
1.3	0.0178	0.0009	0.0012	0.62e-4	1.94
2.1	0.0144	0.0002	0.0013	0.10e-4	1.71
2.7	0.0121	0.0004	0.0012	0.33e-4	1.52
3.5	0.0119	0.0007	0.0012	0.55e-4	1.53
3.8	0.0113	0.0005	0.0011	0.52e-4	1.44

From the results it seems that changing operation point affects the amount of fluctuation present in measured torque estimate  $T_{rms}$ . There is only minor differences in  $n_{rms}$  values. Standard deviation increases in both variables as we are closing the surge region which would suggest that surge might go unnoticed if the  $S$  value is checked only once after the fan has reached a new operation point. However, the calculated RMS values for rotational speed are nearly the same in all of the operation points even when taking the standard deviation into account. For  $T_{rms}$  values there is more variation but it still won't cause the results to overlap when operating near surge region.

Both of the reference values for calculating  $S$  are taken when flow rate  $Q$  is  $3.8 m^3/s$ . This is indicated by having the lowest  $S$  value of  $\sqrt{2}$ . If the only criterion for the reference values is that they are the lowest calculated RMS values, then the references could also be

taken from two separate operation points. As the surge region draws there is an increase in variable  $S$ . In (Tamminen, 2012) threshold for detecting surge was set to be  $S > 2$ . If the same limit is utilized then surging can be detected at one of the operation points which is located inside the surge region.

Filtered values were also tested to see if the  $n_{rms}$  acted differently. Now the rotational speed was filtered with 500 ms time constant which was a default setting for the used VSD. Results in Table 4 represent same operation points as before with unfiltered and filtered speed value taken from them with 20 Hz sampling frequency

Table 4 Surge detection with unfiltered and filtered rotational speed. A single measurement set was taken in each of the operation points with 20 Hz sampling frequency.

<b>Flow rate <math>Q</math> (<math>m^3/s</math>)</b>	<b>Torque variation <math>T_{rms}</math></b>	<b>Unfiltered rotational speed <math>n_{rms}</math></b>	<b>Filtered rotational speed <math>n_{rms, filt}</math></b>	<b>Unfiltered surge detection variable <math>S</math></b>	<b>Filtered surge detection variable <math>S_{filt}</math></b>
0.9	0.0214	0.0009	0.37e-4	2.39	2.42
1.3	0.0168	0.0010	0.34e-4	2.05	1.96
2.1	0.0133	0.0010	0.56e-4	1.77	2.21
2.7	0.0119	0.0010	0.65e-4	1.70	2.26
3.5	0.0113	0.0010	0.64e-4	1.62	2.18
3.8	0.0099	0.0008	0.80e-4	1.41	2.56

Filtered rotational speed has an increase in variation when moving away from the surge region with this sampling frequency. This causes the filtered surge detection variable  $S_{filt}$  to be inconclusive when combined with measured torque variation. Unfiltered result  $S$  has similar values as in Table 3 even though there is only one measurement set taken in each operation point instead of a mean from five measurement sets. This is not unexpected as the standard deviation was low for both  $T_{rms}$  and  $n_{rms}$ . Using filtered variables seems inadvisable, at least if surging is detected from the  $S$  variable. Solely using the filtered speed estimate for surge detection might be possible. Different results could be achieved with alternative sampling frequency or time constant for the filtered parameter.

Same test was repeated with a lower sampling frequency of 1 Hz. Now the parameter monitoring could be done continuously by connecting NETA-21 to the VSD and setting up automatic monitoring with a 5 minute reporting interval. Results from the measurements are presented in Table 5.

Table 5 Surge detection with 1 Hz sampling frequency. Result from unfiltered variables causes  $S$  to have higher threshold for surge detection.  $S > 4$  could be used in this case. Using filtered rotational speed we can see that the amount of variation in  $n_{rms,fil}$  gets higher suddenly which causes surge to be detected at two different operation points.

Flow rate $Q$ ( $m^3/s$ )	Torque variation $T_{rms}$	Unfiltered rotational speed $n_{rms}$	Filtered rotational speed $n_{rms,fil}$	Unfiltered surge detection variable $S$	Filtered surge detection variable $S_{fil}$
0.9	0.0367	0.0007	0.20e-3	4.39	5.71
1.3	0.0156	0.0011	0.36e-3	2.37	7.26
2.1	0.0129	0.0011	0.05e-3	2.15	1.81
2.7	0.0117	0.0011	0.06e-3	2.03	1.84
3.5	0.0111	0.0011	0.06e-3	2.05	1.73
3.8	0.0086	0.0009	0.07e-3	1.59	1.67

Unfiltered rotational speed and torque are behaving similarly to the previous two cases. Variation in torque measurement increases when operating closer to the surge region and  $T_{rms}$  is much higher when operating inside the surge region when sampling is done with low frequency. Using unfiltered values surge can be detected from  $S$  by increasing the threshold for surge detection from  $S > 2$  to  $S > 4$ . When looking at filtered estimates, a sudden increase in  $n_{rms,fil}$  causes surge to be detected at two operation points instead of one. This indicates one false result from the surge detection algorithm when the current operation point is near the surge region. It seems that 1 Hz sampling frequency could be used with either unfiltered or filtered parameters although time constant of the filtered parameters have to be minded.

Overall the surge detection method works with torque and speed estimates provided by the used VSD. Depending on the sampling frequency and the time constant of filter we can use filtered or unfiltered parameter estimates. Results from surge detection with 1 Hz sampling frequency with filtered and unfiltered estimates are also visually presented in Figure 6.4. In this figure,  $S$  values are present as well as the proposed surge detection thresholds for both of the parameter estimates.

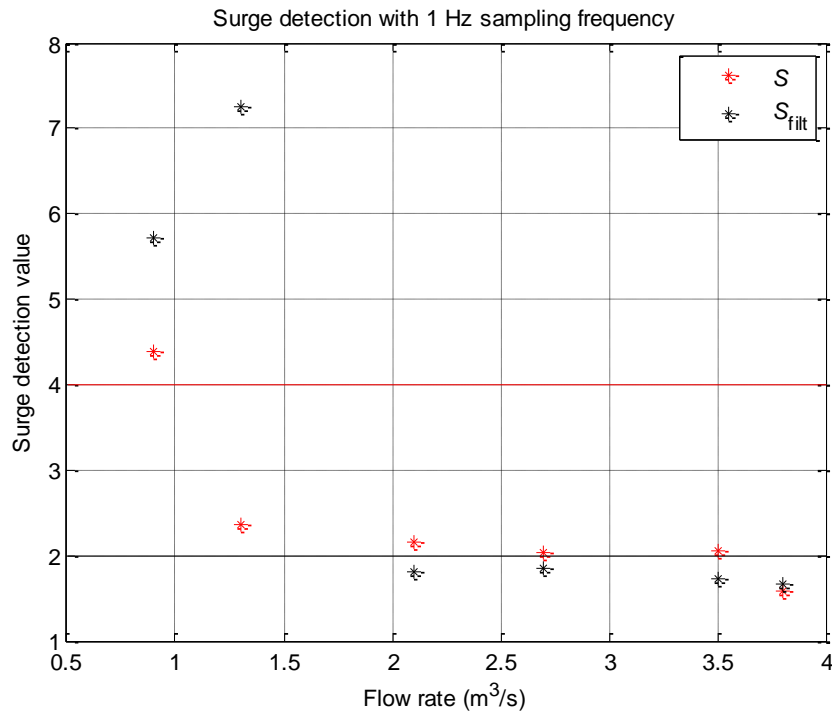


Figure 6.4  $S$ -values from surge detection test with 1 Hz sampling frequency. Low flow rate causes surging after crossing low flow limits of manufacturer's Q-H curve. With filtered rotational speed estimate, we can use surge detection threshold at 2 to notice surging. With unfiltered estimates, the used surge detection threshold should be 3 or 4 instead of 2.

There is a chance for falsely detecting surge in the fan system, as seen from the  $S_{\text{filt}}$  value in Figure 6.4 at the 1.3 m<sup>3</sup>/s flow mark. However in this case it would also indicate that the fan is operating close to the surge region and far away from its best efficiency point.

It is clear that a certain threshold can be set for the  $S$  variable which indicates fan surging. In Figure 6.4 the threshold for filtered estimates is set at 2 and for unfiltered estimates it is set at 4. This threshold depends on at least the monitored parameters, used sampling frequency and filtration.

When using unfiltered speed estimate there is hardly any change in the amount of variation although the lowest results are gained when operating at the edges of the Q-H curve. Monitoring torque estimate or filtered speed and detecting surge solely from them could be a sufficient alternative to the presented method.

In chapter 5.1 an algorithm was introduced to detect areas of steady operation from measurement data. RMS values of torque and rotational speed estimates were calculated from these areas to detect cavitation. If a fan system is being continuously monitored then the same algorithm could be used for surge detection with minor modifications to calculate variable  $S$ . When continuous monitoring is not done, surge can be detected by doing short-term monitoring from time to time with a high sampling frequency, calculating the current  $S$  value and comparing it with a set threshold.

## 6.2 Detecting impeller contamination

Detection of contamination i.e. mass buildup on the fan impeller was tested with a similar method as in (Tamminen, 2013a). Pair of weights were added to the opposite sides of the impeller to increase fan moment of inertia  $J_{\text{Fan}}$ . Combination of bolts, nuts and washers were used to create the additional weights. Two sets of weights were tested, totaling 61g and 141g of additional mass on the impeller. Similar masses were used in (Tamminen, 2013a).

Both of the detection methods presented in the chapter 3.2.3 were tested. When the VSD is operated in a torque control mode, contamination will be detected from the slope of the rotational speed. The additional weight on the impeller decreases angular acceleration of the fan as in equation (10). In a speed control mode, contamination will be detected from a torque integral as in equation (13).

Sampling rate for these detection methods depend on the duration of the fan startup. When the startup takes barely a couple of seconds, a high sampling frequency have to be used since contamination is detected while the torque requirement for fluid transfer is minimal. With equation (12) an upper speed limit for contamination detection in the test system is calculated. Using 0.95 torque ratio  $R_T$  and final rotational speed of the fan  $n_0$  as 800 rpm results to an upper limit of 179 rpm. Utilizing the same 3 % criterion used in (Tamminen, 2013a), a lower speed limit is determined for the system. A nominal speed of 1450 rpm results in a lower limit of 44 rpm. Typical fan startup of the testing setup in speed control mode is presented in Figure 6.5 and in torque control mode in Figure 6.6.

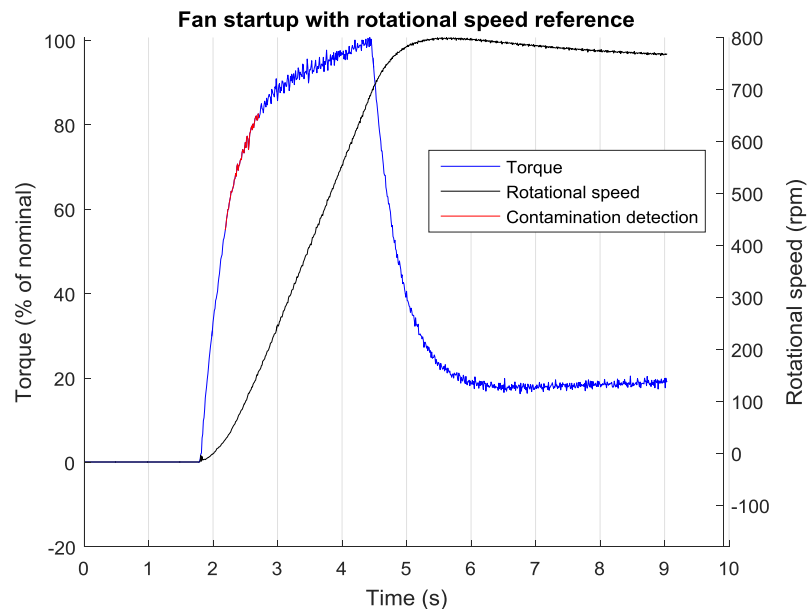


Figure 6.5 Fan startup in speed control mode. Contamination is detected from torque signal. Torque behavior during the startup can vary depending on the speed reference and controller parameters.

From the two methods presented in the chapter 3.2.3 for speed controlled startups, the integrated torque method can be applied with the test system. The first-peak method might be usable with different controller parameters but in the end it is just a special case of the integrated torque method. With the integrated torque method, fan moment of inertia  $J_{\text{Fan}}$

can be calculated from the torque estimates located between the upper and the lower rotational speed limits with

$$J_{Fan} = \frac{\sum_{k=a}^b T(k)\Delta t}{\frac{2\pi}{60}(n_b - n_a)}, \quad (17)$$

where  $b$  and  $a$  are sample indexes,  $n_a$  is the lower speed limit at index  $a$  in a set of rotational speed samples and  $n_b$  is the upper speed limit in the same data set. In this equation torque integral from equation (13) is approximated by using Riemann sum. While  $J_{Fan}$  is calculated with predetermined speed limits and only uses torque samples, both the torque and rotational speed have to be monitored to find the indexes  $a$  and  $b$ . After  $J_{Fan}$  has been calculated for a clean fan impeller it can be used as a reference point for future monitoring to notice a mass increase and contamination buildup.

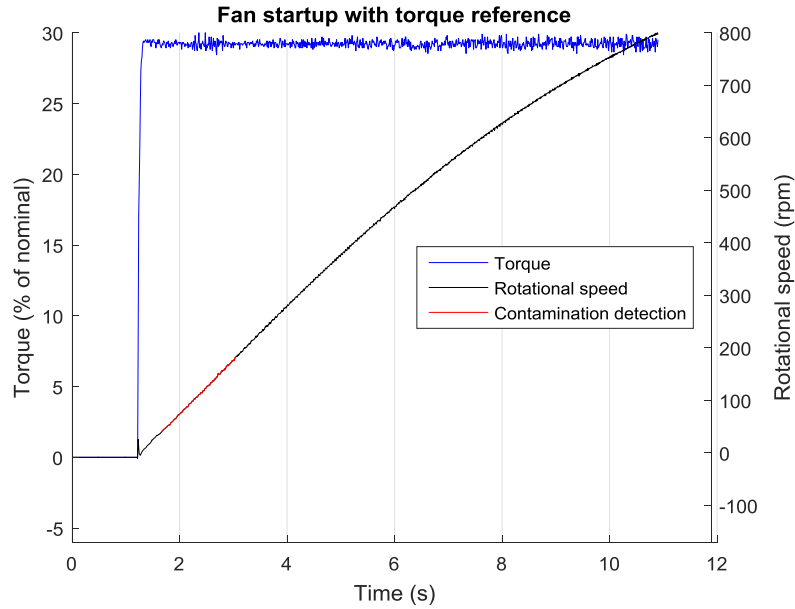


Figure 6.6 Fan startup in torque control mode. Impeller contamination is detected from the slope of the rotational speed. Contamination buildup reduces angular acceleration when constant torque is applied resulting in a gentler slope.

When using a constant torque reference for fan startup, the rotational speed increases linearly at the beginning of the startup. This represents a constant angular acceleration. Determining the angular acceleration during this time allows noticing of a change in the fan moment of inertia as in equation (10). When the typical acceleration with a clean fan impeller is known, increase in the fan moment of inertia  $\Delta J_{Fan}$  can be calculated with

$$\Delta J_{Fan} = \frac{T_{ref}}{\omega_{ref} - \omega_{current}}, \quad (18)$$

where  $T_{ref}$  is a torque reference used in the startup,  $\omega_{ref}$  is a constant angular acceleration when operating with a clean fan impeller and  $\omega_{current}$  is a constant angular acceleration measured from the most recent fan startup.

Change in the fan moment of inertia  $\Delta J_{Fan}$  can be used to estimate the level of

contamination on the impeller. The actual amount of excess mass can be derived from equation of moment of inertia of a thick-walled cylindrical tube

$$\Delta m = \frac{2\Delta J_{Fan}}{r_1^2 + r_2^2}, \quad (19)$$

where  $r_1$  is the inner radius and  $r_2$  is the outer radius of the cylinder which centers at the rotating axis (Tamminen, 2013a). The extra masses used in testing were attached at a distance of half of the fan diameter from the rotating axis, resulting in  $r_1 = r_2 = 0.315$  m. Now equation (19) can be simplified for the testing setup to

$$\Delta m = \frac{\Delta J_{Fan}}{0.315^2}. \quad (20)$$

From Figure 6.5 and Figure 6.6 we can see that the area of interest, from which the angular acceleration is determined during a fan startup, is passed in less than a second. To get enough data samples, torque and rotational speed were monitored with a 100 Hz sampling frequency by using DCP. Sampling frequency should be high to get accurate results from a fast fan startup but due to the data logger buffer size a higher frequency was not practical as it limited the overall sampling time too much.

Table 6 Results from contamination detection test. Fan startup was monitored and two methods were applied for noticing contamination buildup depending on the used control mode.

<b>Additional weight</b>	<b>Torque control mode, <math>J_{Fan}</math> (<math>\text{kgm}^2</math>)</b>	<b>Speed control mode, <math>J_{Fan}</math> (<math>\text{kgm}^2</math>)</b>	<b>Torque control mode, <math>\Delta m</math> (g)</b>	<b>Speed control mode, <math>\Delta m</math> (g)</b>
0g	1.4642	1.3318	0	0
61g	1.4768	1.3235	-58.2	-83.4
141g	1.4584	1.3442	127.7	124.6

Table 6 shows the results of contamination detection test. For each weight set, the fan system was started five times in both torque and speed control mode and the average moment of inertia was calculated. With equation (19) the difference in mass was estimated. When 61 g of extra weight was added to the impeller, both of the detection methods produced vastly erroneous mass estimates. This might be due to the used sampling frequency or too low amount of added extra mass but the exact reason for this is not known. With 141 g of added weight, the results from the detection methods indicated a mass increase and the estimated mass increase was circa 90 % of the actual added mass.

A better way to conduct the contamination detection test could have been adding smaller amounts of mass to simulate real, slow mass buildup and gradually detect the mass increase as was seen in (Tamminen, 2015). With the current results, it seems that the mass increase is noticeable with VSD after a certain amount of mass compared to the fan weight has been accumulated on the impeller surface. Inaccurate predictions were also present in (Tamminen, 2015) but when calculating a trend line from the estimated mass increases, the detection method worked properly over a longer period of time.

When utilizing sensorless contamination detection, sampling rate should be considered based on the actual startup time of the fan. High sampling frequency is always advisable. Data logger's buffer size should also be taken into consideration when deciding on sampling frequency. If the buffer size is limited some compromises have to be made for the used sampling frequency. Results from the contamination detection tests show that fan impeller contamination can be noticed regardless of the used control mode although the integrated torque method requires more computations. With more excess mass on the impeller, applicability of the detection methods increases. Small amount of contaminants might be completely unnoticeable.

## 7 INDUSTRIAL PILOT: DETECTING CAVITATION FROM PUMPS USED IN PAPER MILLING

Sensorless cavitation detection was tested in an industrial pilot experiment. Cavitation had been previously noticed from impeller damages at a paper mill. Methods presented in this thesis were applied to remotely monitor occurrence of cavitation in two different pumping systems. Parameter estimates were continuously monitored from 31.5.2016 to 11.6.2016 by using 1 Hz sampling frequency. This frequency was deemed sufficient for sensorless cavitation detection in chapter 5 through testing in laboratory environment. Measurement data was presented in XML formatted reports that were created once a minute. Figure 7.1 shows a part of a measurement file.

```
<signal unit="rpm" scale="0" timestamp="2016-05-31T15:15:16.119" name="02_01_02_speed" value="839.124756"/>
<signal unit="" scale="0" timestamp="2016-05-31T15:15:16.264" name="02_162_05_IGBT_Temp_C" value="48.749207"/>
<signal unit="" scale="0" timestamp="2016-05-31T15:15:16.320" name="02_162_06_IGBT_Temp_J" value="59.67009"/>
<signal unit="%" scale="0" timestamp="2016-05-31T15:15:21.046" name="02_01_05_torque" value="39.094223"/>
<signal unit="rpm" scale="0" timestamp="2016-05-31T15:15:21.089" name="02_01_02_speed" value="839.321411"/>
<signal unit="" scale="0" timestamp="2016-05-31T15:15:21.236" name="02_162_05_IGBT_Temp_C" value="48.792007"/>
<signal unit="" scale="0" timestamp="2016-05-31T15:15:21.293" name="02_162_06_IGBT_Temp_J" value="59.888367"/>
<signal unit="%" scale="0" timestamp="2016-05-31T15:15:26.062" name="02_01_05_torque" value="38.067596"/>
<signal unit="rpm" scale="0" timestamp="2016-05-31T15:15:26.110" name="02_01_02_speed" value="839.319092"/>
<signal unit="" scale="0" timestamp="2016-05-31T15:15:26.248" name="02_162_05_IGBT_Temp_C" value="48.747658"/>
<signal unit="" scale="0" timestamp="2016-05-31T15:15:26.307" name="02_162_06_IGBT_Temp_J" value="59.484009"/>
<signal unit="%" scale="0" timestamp="2016-05-31T15:15:31.093" name="02_01_05_torque" value="38.093575"/>
<signal unit="rpm" scale="0" timestamp="2016-05-31T15:15:31.139" name="02_01_02_speed" value="839.174805"/>
<signal unit="" scale="0" timestamp="2016-05-31T15:15:31.283" name="02_162_05_IGBT_Temp_C" value="48.712013"/>
<signal unit="" scale="0" timestamp="2016-05-31T15:15:31.339" name="02_162_06_IGBT_Temp_J" value="59.594513"/>
<signal unit="%" scale="0" timestamp="2016-05-31T15:15:36.076" name="02_01_05_torque" value="38.030556"/>
<signal unit="rpm" scale="0" timestamp="2016-05-31T15:15:36.122" name="02_01_02_speed" value="839.540771"/>
```

Figure 7.1 Part of a measurement report in XML format. While the report contains multiple parameters, only torque and rotational speed are extracted for further analysis.

An analysis script was created with Matlab to collect the required data for cavitation detection from the report files. Amongst all of the measured parameters, torque and rotational speed were looked up alongside their reference values. The measurement data was gathered from two different VSDs referred to as VSD<sub>1</sub> and VSD<sub>2</sub>. Detection of steady state operation was done from the torque data to find areas from which cavitation could be detected. After finding these areas, RMS values were calculated for both torque and rotational speed estimates. Following figures present the gathered torque and speed data from the two VSDs as well as the results from the cavitation detection method. Areas of recognized steady operation are marked with red.

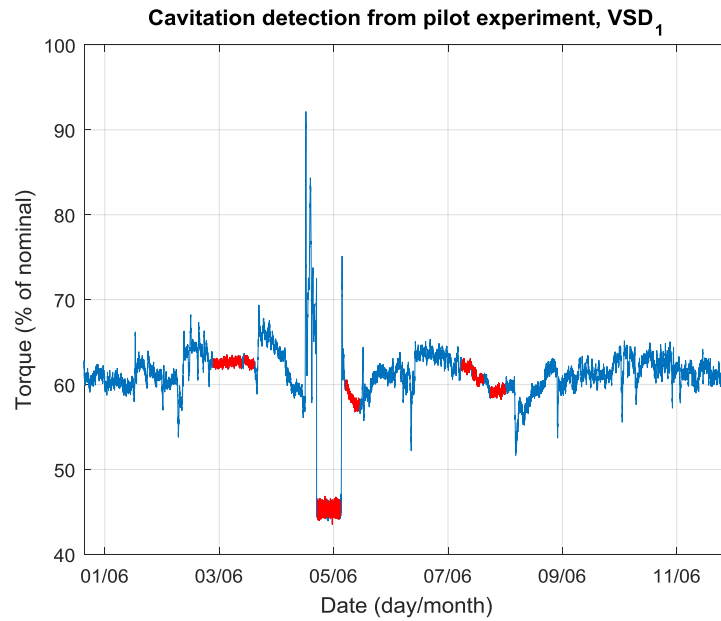


Figure 7.2 Torque estimates provided by the VSD<sub>1</sub>. Several areas of constant operation were detected (marked with red) even with such high variety in torque.

Torque estimate varies greatly in the data provided by the VSD<sub>1</sub> when looking at almost two weeks' worth of measurement data at once. Between June 4<sup>th</sup> and 6<sup>th</sup> there is a visually noticeable increase in the variation amplitude during a recognized steady state operation.

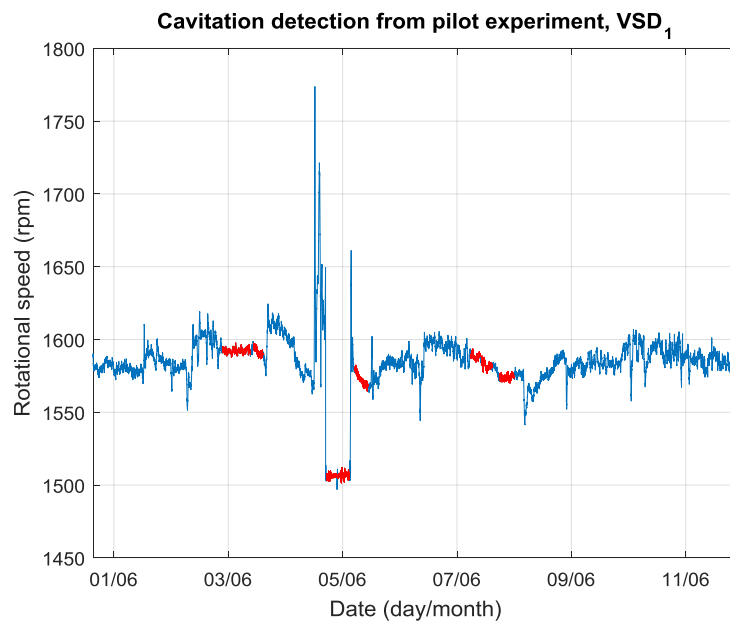


Figure 7.3 Rotational speed estimates provided by VSD<sub>1</sub>. Areas of constant operation were detected from torque data.

Variation amplitude during steady state operation is a lot more similar between all of the recognized steady areas. This makes cavitation detection from the rotational speed estimates unlikely. Results of cavitation detection method are presented in Table 7.

Table 7 Cavitation detection from pumping process controlled by VSD<sub>1</sub>. The lowest calculated RMS values are used as reference points when comparing RMS values.

Starting time of steady state operation	Variation in torque $T_{rms}$	Ratio between reference and current value $T_{ref}/T_{rms}$	Variation in rotational speed $n_{rms}$	Ratio between reference and current value $n_{ref}/n_{rms}$
02/06 21:33	0.0038	1.1118	0.0009	1.5978
03/06 10:37	0.0034	1.0000	0.0009	1.5980
04/06 17:16	0.0070	2.0616	0.0006	1.0000
04/06 22:03	0.0072	2.1444	0.0010	1.6795
05/06 05:02	0.0052	1.5377	0.0009	1.5455
07/06 05:43	0.0046	1.3650	0.0010	1.7248
07/06 10:22	0.0062	1.8465	0.0012	2.1344
07/06 17:59	0.0046	1.3635	0.0009	1.6094
11/06 19:07	0.0039	1.1636	0.0009	1.6100

When using 2 as the threshold ratio for cavitation detection between reference and current RMS values, cavitation is detected on June 4<sup>th</sup> from torque data. Looking at the Figure 7.2, there is a clearly seen increase in the signal's variation amplitude during this time period which indicates that the cavitation detection has been successful. On the other hand rotational speed surpasses the threshold limit on June 7<sup>th</sup>. On this area the amount of variation has not significantly increased in either of the signals. This result may be because the actual parameter value is slowly decreasing but it is still recognized as a steady area. This can be solved by either improving the steady state recognition algorithm or handling the data in smaller sized segments, e.g. data from one day at a time so that the input parameters of the steady state recognition algorithm can be adjusted accordingly.

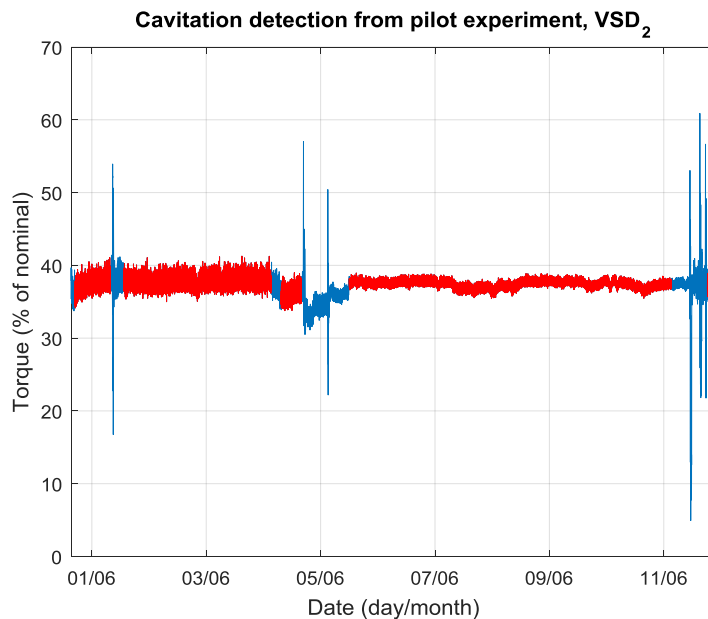


Figure 7.4 Torque estimates provided by VSD<sub>2</sub>. Areas of steady operation are marked as red.

The second pumping process operates overall more steadily than the first which makes the detection of steady operation areas easier. There is a noticeable decrease in the variation

amplitude after June 5<sup>th</sup> when the steady state operation proceeds. This could indicate presence of cavitation before June 5<sup>th</sup>.

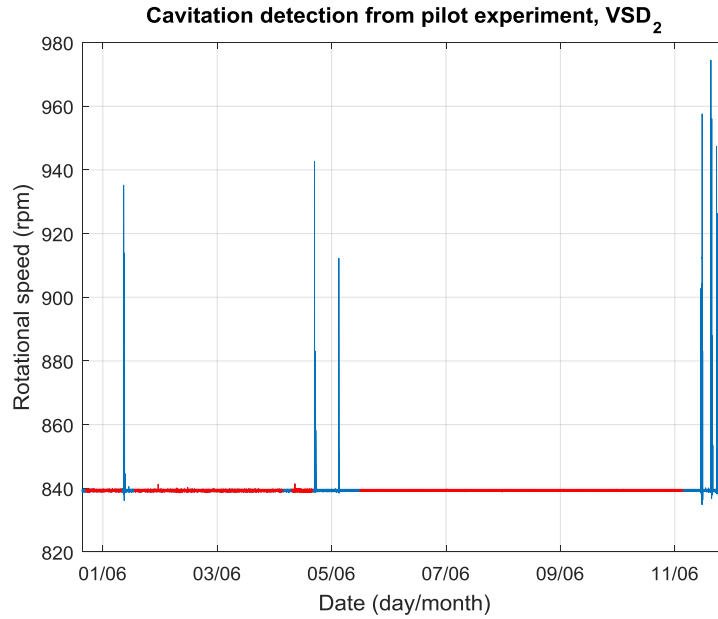


Figure 7.5 Rotational speed estimates provided by VSD<sub>2</sub>. Areas of constant operation are found from the torque data of the VSD<sub>2</sub>.

Since there are a couple of high rpm values, this figure does not clearly show the difference in variation between the steady operation areas. However results from cavitation detection method show that the RMS values behave similarly than the ones calculated from the torque estimates. After June 5<sup>th</sup> when there is a reduction in variation amplitude as seen from the torque estimates, the RMS value of the rotational speed signal also decreases.

Table 8 Cavitation detection from pumping process controlled by VSD<sub>2</sub>. The lowest calculated RMS values are used as reference points for detecting cavitation.

Starting time of steady state operation	Variation in torque $T_{rms}$	Ratio between reference and current value $T_{ref}/T_{rms}$	Variation in rotational speed $n_{rms}$	Ratio between reference and current value $n_{ref}/n_{rms}$
31/05 16:55	0.0175	1.4732	0.1458	1.2871
01/06 13:15	0.0162	1.3621	0.1428	1.2598
04/06 07:30	0.0178	1.5008	0.1485	1.3105
05/06 21:01	0.0119	1.0000	0.1133	1.0000
11/06 18:19	0.0134	1.1283	0.1393	1.2297

Although the increase in variation amplitude is clearly visible in the figures, threshold ratio of 2 for cavitation detection is not reached. This may be because of the used reference value is too high to represent pump running in optimal conditions or the threshold ratio is too high and should be adjusted accordingly. Ultimately, some change has happened in the monitored pumping process as there is such a clear change seen in the signal's variation amplitude and calculated RMS values even when the operation point has not changed. One possibility could be a change in temperature of the pumped fluid which would affect the vapor pressure and NPSH<sub>a</sub>.

Cavitation had been previously noticed at the mill from impeller damages. Applying sensorless cavitation detection methods allows more precise detection of when the cavitation has occurred. This information could be used to eliminate the cavitation conditions if possible, as the cause of the cavitation can be tracked down from the timing, or to monitor the overall time the pumping system has been cavitating and deriving the need for equipment maintenance from there. There are still two key issues with the cavitation detection method; namely finding the suitable reference values and threshold ratios. If the reference RMS values are gained by continuously monitoring the pumping process and choosing the lowest calculated values, then the threshold value might have to be adjusted to suit the process if the pump is never run in its optimal operation region.

## 8 SUMMARY AND CONCLUSIONS

Currently there exists multiple fluid handling systems that are being utilizing energy inefficiently. Oversizing is a common problem in pump and fan systems, an issue which has been resolved with control methods such as throttling to get the desired flow rate. Retrofitting a better control method can be costly but overall during the system's lifetime it can reduce the total LCC due to the savings in energy consumption. VSDs are greatly beneficial to pump and fan applications in terms of efficient usage. While providing a better way to control the fluid's flow rate in a system, there are also other uses that can provide more value out of them. When considering system monitoring, traditional sensors are usually installed, which brings forth additional costs such as the initial investments, installations and maintenance. Alternatively VSDs can be used as monitoring tools to detect deleterious phenomena such as cavitation, impeller contamination, surging and component breakage. Provided that a VSD is equipped with its own data logger, sensorless system monitoring can be realized solely by monitoring a couple of key parameter estimates provided by the VSD. Remote monitoring is also a considerable possibility if the collected data can be accessed and processed off-site.

In this thesis the usability of a VSD as a tool for sensorless fluid system monitoring was tested. Data logging was done either directly with a VSD or the required parameter estimates were provided by the VSD to an external remote monitoring tool NETA-21 or DCP program. Occurrences of deleterious phenomena in pump and fan systems were remotely monitored by having an access to the measurement files and analyzing the data with Matlab.

### 8.1 Sensorless detection methods

Sensorless detection methods were tested with two different fluid system setups. One test setup for a centrifugal pumping system which could be used for cavitation detection and noticing NRV breakdown and one setup for a radial fan blower system for surge detection and noticing contamination buildup on a fan impeller surface. Operation points of both of these systems were controlled by throttling at the discharge sides. Current operation point for pump was estimated from flow, pressure and power measurements. With the fan system, flow and power measurements were used to determine the current operation point.

The first deleterious phenomenon handled in this thesis was cavitation which causes damage to the pumping equipment due to bubble implosions. It increases maintenance costs of a pumping system prone to cavitation. System's overall energy efficiency is also reduced as cavitation is often a sign that the system operates outside of its best operating region. Detection of cavitation was done by monitoring torque and rotational speed estimates and calculating RMS value of their variations. Higher variation in the measured signals indicated possible flow recirculation and cavitation. At the very least the increased variation was a sign of operating outside of the pump's best efficiency region. This detection method has a prerequisite of knowing reference behaviour of the pump when it's operating at the BEP or at least near it. Reference behaviour could be monitored and stored with a separate test run if possible. Otherwise it is more difficult to gauge the actual reference behaviour. In such situations the pumping system can be continuously monitored and the lowest measured RMS value can be used as the reference point when detecting cavitation. After estimating the reference RMS values for torque and rotational speed, the

pump was run at different operating points, decreasing flow rate step-by-step and getting closer to the cavitation conditions. The results show that even with a sampling frequency of 1 Hz cavitation is detectable from the VSD's filtered speed and torque estimates. After confirming the required sampling rate, NETA-21 was used to continuously monitor the pumping system with 1 Hz sampling frequency during a test run which involved multiple operation points. A Matlab script was developed to automatically notice areas where the pump was operating steadily. From these areas the script calculated RMS values for torque and speed estimates and detected cavitation. The results showed that this type of remote monitoring could be used for cavitation detection. This method was later on applied in a real-life pilot experiment.

Possibility to notice equipment breakdown was studied in terms of monitoring condition of a NRV at the pump discharge. NRVs are used to prevent reverse flow and as such they are critical parts in fluid handling systems. Sensorless NRV condition monitoring was done by comparing shutdown behaviour of a pumping system with a working NRV and with a faulty i.e. open NRV. VSD's torque estimate behaves differently when there has been malfunction in the NRV as the motor has to provide excess torque to realize the desired shutdown behaviour and to prevent a reverse rotation due to the return flow. Results from laboratory tests indicate that monitoring shutdown behaviour of a pumping system with a VSD could be used to detect a NRV breakdown. Minor leakage and incipient breakdown could be more difficult to notice but further study on the topic would be required to confirm this. A complete NRV breakdown is detectable with parameter estimates provided by a VSD.

Fan surging occurs when there is too low flow rate in a fan system. It causes pressure drops and oscillations which can lead to a flow reversal in the fan system. Surge can be detected similarly to cavitation, from the low frequency fluctuations in torque and rotational speed signals. Similarly to the cavitation detection method, reference behaviour needs to be known and surge is detected by comparing current calculated RMS values of the signal variations with reference behaviours. Surge detection method was tested with an axial fan system having a damper at the fan discharge side to move the current operation point towards the surge conditions. Results from the tests showed that surge can be detected from VSD's torque and rotational speed estimates. It could be possibly to notice surge just from the torque estimate, as the increase in surge detection variable  $S$  consisted mostly of the increase in RMS value of torque  $T_{\text{rms}}$ . If the monitored parameters are pre-filtered by the VSD then low sampling frequency is required. The used sampling frequency could be as low as 1 Hz. When data logging is done with a higher frequency, using unfiltered estimates is necessary for the detection method to work.

Detection of contamination buildup on a fan impeller can be cause of a fan system failure. Periodic maintenance is required to keep the impeller clear of contaminants. The maintenance should be done when necessary to avoid excess system downtime and costs. Thus monitoring impeller contamination is required. Sensorless detection method of impeller contamination was based on increased fan moment of inertia caused by the mass of contaminants. In the testing environment, contamination buildup was simulated by adding extra weight on the opposite sides of the fan impeller. Contamination was monitored from the torque and rotational speed estimates provided by the used VSD. Two detection methods were tested, one for a fan system used in torque control mode and one for a speed controlled system. Since the mass detection is done during the fan startup, the

used sampling frequency is situational depending on the limitations of the used hardware and the startup time of the fan. Fan startup tests showed that the impeller contamination can be detected by using the VSD's parameter estimates. As the fan is used over time, more and more extra mass adhere to the impeller surface. Contamination detection method seems to give more accurate results with higher levels of contamination. Small amounts of contaminants might go unnoticed or produce incorrect results.

## **8.2 Pilot experiment**

Cavitation detection method was tested in an industrial pilot experiment. Cavitation had been detected at a paper mill from the condition of impeller surfaces. Sensorless cavitation detection method was applied and occurrences of cavitation during pumping processes were remotely monitored from the data gathered by two VSDs. Continuous measurement data was gathered continuously during 31.5.2016-11.6.2016 with 1 Hz sampling frequency. Cavitation was detected from the pumping processes with the sensorless detection method. Possible issues with the applied cavitation detection method are finding the correct reference values, finding the threshold ratio which indicates cavitation and highly varying torque and rotational speed which makes recognition of operation states more difficult.

## **8.3 Final thoughts**

The amount of information that can be extracted from a modern VSD is immense. Most of the commercially available VSDs are able to provide estimates for various parameters such as power, torque and rotational speed. These can be used to monitor usage and trends but also system conditions, providing insight on the current state of the system and appearance of deleterious phenomena. This can reduce the amount of required external sensor and measuring equipment, leading to more cost-efficient and better utilization of VSD in fluid handling systems. There is still a need for testing and development of different system monitoring methods to find out which of them are suitable for end-use and how they should be implemented for efficient usage.

## REFERENCES

- (ABB, 2013) ABB, *ABB industrial drives – ACS880, single drives 0.55 to 560 kW – Catalog*, 2013. Available at: [http://www.simarkcontrols.com/pdf/abb/ACS880\\_SingleDrives.pdf](http://www.simarkcontrols.com/pdf/abb/ACS880_SingleDrives.pdf)
- (ABB, 2014) ABB, *User's manual – NETA-21 remote monitoring tool*, 2014. Available at: [https://library.e.abb.com/public/5ad2a0e9056a171ec1257dc800390dfa/NET\\_A\\_21-UM\\_revD\\_screen\\_A4.pdf](https://library.e.abb.com/public/5ad2a0e9056a171ec1257dc800390dfa/NET_A_21-UM_revD_screen_A4.pdf)
- (ABB, 2015) ABB, *NETA-21 Remote monitoring tool firmware 2.26. Update to 2.26.0.0*, 2015. Available at: <http://www.abb.com/abblibrary/DownloadCenter/?CategoryID=9AAC159480&View=Result>
- (Aerovent, 2012) Aerovent, *Surge, stall and instabilities in fans*, 2012. Available at: <http://www.aerovent.com/docs/fan-engineering-topics/surge-stall-and-instabilities-in-fans---fe-600.pdf>
- (Ahonen, 2011a) Ahonen T., Tamminen J., Ahola J. & Kestilä J., *Novel method for detecting cavitation in centrifugal pump with frequency converter*, *Insight – Non-Destructive Testing and Condition Monitoring*, Volume 53 Number 8, August 2011, pp. 439-449. Available at: <http://www.ingentaconnect.com/content/bindt/insight/2011/00000053/0000008/art00008>
- (Ahonen, 2011b) Ahonen T., *Monitoring of centrifugal pump operation by a frequency converter*, Yliopistopaino, Lappeenranta, 2011, ISBN: 978-952-265-075-7
- (Ahonen, 2015) Ahonen T., Tamminen J., Ahola J. & Saukko J., *Monitoring of Non-Return Valve Operation with a Variable-Speed Drive*, IEEE, 17<sup>th</sup> European Conference on Power Electronics and Applications, September 2015, DOI: 10.1109/EPE.2015.7309204
- (Almeida, 2003) de Almeida A.T, Fonseca P., Falkner H. & Bertoldi P., *Market transformation of energy-efficient motor technologies in the EU*, *Energy Policy* 31, 2003, pp. 563-575
- (Al-Khalifah, 2013) Al-Khalifah M. & McMillan G., *Control valve versus variable-speed drive for flow control*, *InTech Magazine*, July/August 2013. Available at: <https://www.isa.org/standards-and-publications/isa-publications/intech-magazine/intech-archives-2013/#2013-jul-aug>
- (Badr, 2015) Badr H.M. and Ahmed W.H., *Pumping machinery theory and practice*, Wiley, 2015, pp. 159-197, ISBN: 978-1-118-93208-7
- (BEE, 2004) Bureau of Energy Efficiency (BEE), Government of India. *Energy Efficiency in Thermal Utilities*, 2004, Chapter 5, pp. 93-112. Available at: <https://beeindia.gov.in/content/energy-auditors>
- (Brennen, 1994) Brennen C.E., *Hydrodynamics of pumps*, Concepts ETI & Oxford University Press, 1994, ISBN: 0-933283-07-5 (Concepts ETI) & 0-19-856442-2 (Oxford University Press)
- (CLIC, 2016) CLIC Innovation, *EFEU – Efficient energy use*, 2016. Available at: <http://clicinnovation.fi/activity/efeu/>

- (Drydock, 2003) Drydock magazine, *Cutting the Cost of Cavitation*, December 2003, pp. 32-34. Available at: <http://www.drydockmagazine.com/previous-magazines/>
- (Eaton, 2016) Eaton, *SPX9000 High performance*, 2016. Available at: <http://www.eaton.com/Eaton/ProductsServices/Electrical/ProductsandServices/AutomationandControl/AdjustableFrequencyDrives/IndustrialDrives/SPX/index.htm>
- (Eldridge, 2016) Eldridge Products, *Master-Touch™ Series 9800MPNH Flowmeters*, 2016. Available at: [http://www.epiflow.com/files/Series\\_9800MPNH.pdf](http://www.epiflow.com/files/Series_9800MPNH.pdf)
- (Emotron, 2016) Emotron, *Emotron M20 shaft power monitor*, 2016. Available at: <http://www.emotron.com/products-solutions/products/shaft-power-monitors/m20/>
- (Evans, 1996) Evans R., Sneed R. E. & Hunt J. H., *Pumping Plant Performance Evaluation*, North Carolina Cooperative Extension Service, Publication number: AG 452-6, 1996. Available at: <https://www.bae.ncsu.edu/extension/extension-publications/water/irrigation/ag-452-6-pumping-plant-evans.pdf>
- (Fläkt Woods, 2015) Fläkt Woods, *Calculation of Life Cycle Costs for Air Handling Units*, Fläkt Woods Group, 2015. Available at: <http://www.flaktwoods.co.uk/support-centre/im-a-designer/life-cycle-cost-for-ahus/>
- (Fläkt Woods, 2015) Fläkt Woods, *Industrial Centripal Fans: Centripal EU*, Fläkt Woods Group, 2016. Available at: <http://www.condair.nl/m/0/ventilator-fl-ktwoods-centripal-eu-brochure.pdf>
- (Forsthoffer, 2005) Forsthoffer W.E, *Forsthoffer's Rotating Equipment Handbooks Vol 2: Pumps*, Elsevier Science & Technology Books, 2005, pp. 85–107, ISBN: 1856174689
- (Grundfos, 2004) Grundfos, *Pump handbook*, GRUNDFOS Management A/S, 2004. Available at: <http://net.grundfos.com/doc/webnet/mining/downloads/pump-handbook.pdf>
- (Grundfos, 2009) Grundfos, *The Centrifugal Pump*, GRUNDFOS Management A/S, 2009
- (Grundfos, 2016) Grundfos, *E-solutions with Grundfos e-pumps*, GRUNDFOS Management A/S 2016. Available at: <http://net.grundfos.com/App/WebCAPS/Grundfosliterature-1398449.pdf>
- (HI, 2001) Hydraulic Institute, Europump and U.S. Department of Energy Office of Industrial Technologies, *Pump Life Cycle Costs – A Guide to LCC Analysis for Pumping Systems, Executive Summary*, January 2001, p. 19, DOE/GO-102001-1190
- (HI, 2004) Hydraulic Institute, Europump and U.S. Department of Energy Industrial Technologies Program, *Variable Speed Pumping – A Guide to Successful Applications, Executive Summary*, May 2004, p. 22, DOE/GO-102004-1913
- (Holtz, 2000) Holtz J., *Sensorless Control of Induction Motors – Performance and Limitations*, Proceedings of the 2000 IEEE International Symposium on Industrial Electronics, 2000
- (Huoman, 2015) Huoman K., *Fan system monitoring via cloud service*, Lappeenranta, 2015

- (ITT, 2016) ITT, *Load monitors*, 2016. Available at: <http://www.ittproservices.com/aftermarket-products/control/ps10-and-ps20-load-monitors/>
- (Karassik, 1976) Karassik I.J., Krutzsch W.C., Fraser W.H. and Messina J.P., *Pump handbook*, McGraw-Hill, 1976, pp. 2-144 – 2-160, ISBN: 0-07-033301-7
- (Karassik, 1998) Karassik I.J and McGuire T., *Centrifugal pumps*, Chapman & Hall, USA, 1998
- (Orkisz, 2008) Orkisz M., Wnek M., Kryczka K. and Joerg P., *Variable Frequency Drive as a Source of Condition Monitoring Data*, International Symposium on Power Electronics, Electrical Drives, Automation and Motion, 2008
- (Pump World, 2014) Pump World, *Centrifugal pump discharge cavitation*, 2014. Available at: <http://www.pumpworld.com/centrifugal-pump-discharge-cavitation.htm>
- (Pöyhönen, 2016) Pöyhönen S., *Variable-speed-drive-based detection methods for problems in fluid handling systems*, Lappeenranta, 2016. Available at: <http://urn.fi/URN:NBN:fi-fe2016051612389>
- (Lins, 2014) Lins C., Williamson L., Leither S. & Teske S., , *10 Years of renewable energy progress*, Renewable energy policy network for the 21<sup>st</sup> century, 2014, ISBN: 978-3-9815934-4-0. Available at: [http://www.ren21.net/Portals/0/documents/activities/Topical%20Reports/REN21\\_10yr.pdf](http://www.ren21.net/Portals/0/documents/activities/Topical%20Reports/REN21_10yr.pdf)
- (Schiavello, 2009) Schiavello B. and Visser F. C., *Pump cavitation – various NPSHR criteria, NPSHA margins and impeller life expectancy*, Proceedings of 25th International Pump Users Symposium, Houston, USA, February 2009, pp 113-144
- (SDA, 2016) SD Association, *Capacity (SD/SDHC/SDXC)*, 2016. Available at: <https://www.sdcard.org/developers/overview/capacity/>
- (Taco, 2013) Taco, *Introducing the Taco SelfSensing Series With ProBalance<sup>tm</sup>*, 2013. Available at: <https://www.taco-hvac.com/news.html?News=848>
- (Tamminen, 2012) Tamminen J., Ahonen T., Ahola J., Jaatinen A. and Røyttä P., *Sensorless method for detecting surge in variable-speed-driven fan systems*, CM & MFPT, London, UK, June 2012, CD-ROM
- (Tamminen, 2013a) Tamminen J., Ahonen T., Ahola J., Niemelä M., Tahvanainen A. & Potinkara A., *Detection of Mass Increase in a Fan Impeller With a Frequency Converter*, IEEE Transactions on industrial electronics, VOL. 60, NO. 9, September 2013
- (Tamminen, 2013b) Tamminen J., *Variable speed drive in fan system monitoring*, Yliopistopaino, Lappeenranta, 2013, ISBN: 978-952-265-532-5
- (Tamminen, 2015) Tamminen J., Ahonen T., Ahola J., Pöyhönen S. & Tiainen T., *Variable Speed Drive-Based Fan Impeller Contamination Build-Up Detection: Industrial Case Study*, 17<sup>th</sup> European Conference on Power Electronics and Applications, 8-10 September 2015, DOI: 10.1109/EPE.2015.7309287
- (US EERE, 2003) U.S. Department of Energy Efficiency and Renewable Energy, *Improving Fan System Performance – A Sourcebook for Industry*, April 2003, p. 32, DOE/GO-102003-1294

- (Volk, 2005) Volk M., *Pump Characteristics and Applications – Second Edition*, Taylor & Francis Group, 2005, ISBN: 978-0-82472-755-0
- (Wikipedia, 2006) Wikipedia, *Cavitation damage evident on the propeller of a personal watercraft*, 2006. Available at: [https://commons.wikimedia.org/wiki/File:Cavitation\\_Propeller\\_Damage.JPG](https://commons.wikimedia.org/wiki/File:Cavitation_Propeller_Damage.JPG)
- (Wilson, 2005) Wilson J. S., *Sensor Technology Handbook*, Elsevier, 2005, ISBN: 0-7506-7729-5
- (Xylem, 2016) Xylem, *Flygt PumpSmart, PS200*, 2016. Available at: <http://www.xylemwatersolutions.com/scs/uk/en-gb/brands/flygt/Monitoring%20and%20control/pumpdrives/pumpsmart/Documents/Flygt%20PumpSmart%20Xylem.pdf>